Universidade de Lisboa
Faculdade de Ciências
Departamento de Física

Test bench for testing performances of Silicon Ball detector array at CMAM

David Santinhos Ferreira

Mestrado Integrado em Engenharia Física

Dissertação orientada por: Professor Doutor Daniel Galaviz Redondo
e Professor Doutor Ángel Miguel Sánchez Benitez

2016

Aos meus pais Florbela e Amílcar, à minha irmã Inês que me ajudaram neste percurso a ultrapassar muitos obstáculos e sempre me apoiaram. Aos meus amigos de longa data que estiveram sempre presentes. Aos meus colegas de faculdade, aos professores e a todos aqueles que me apoiaram nestre trajecto da minha vida. Em geral a todas as pessoas que sempre que precisei estavam presentes. A todos um MUITO OBRIGADO.

"Recomeça
Se puderes,
Sem angústia e sem pressa.
E os passos que deres,
Nesse caminho duro
Do futuro,
Dá-os em liberdade.
Enquanto não há alcances,
Não descanses.
De nenhum fruto querias só metade."

Miguel Torga

Abstract

The Silicon Ball (Si-ball) is a semi-conductor based detector developed and constructed at ISOLDE-CERN. It was exploited for more than a decade at ISOLDE-CERN to experimentally investigate static and dynamic properties of exotic nuclei which are produced by means of the ISOL-technique. Due to some technical limitations at the time, the detector was moved to the Centre for *Micro Analysis of Materials* (CMAM) in Madrid, Spain.

CMAM is a multidisciplinary laboratory in which different ion beams of stable nuclei are nowadays produced with a 5 MV Tandem accelerator in combination with two different ion sources. Traditionally, one of the research lines of this laboratory was devoted to fundamental nuclear science, where recently low energy reactions relevant for nuclear astrophysics have been measured.

The aim of my Master Thesis is the adaptation and start-up of the recently brought Si-ball charged particle detector at the nuclear physics line of the CMAM, preparing it for future campaigns of experiments devoted to investigate a variety of aspects on the structure and dynamics of the atomic nucleus.

During my stay in Madrid, I worked within a collaborative framework that made it possible for interaction with experienced scientific and technical staff. The work involved developments at the level of electronic instrumentation and the execution of experiments aiming at characterizing the Silicon detectors and its electronic chain. Several integrated electronic components were considered, as well as data acquisition, treatment and analysis software. In addition, the work covered aspects of vacuum technology, beam diagnostic systems in particle accelerators, high granularity solid states detectors or integrated electronics. The main task in which I was already directly involved was the energy calibration of the Si-ball Silicon detectors using several alpha particle radioactive sources, and the determination of the dead layer thickness of each working units of Si-ball.

Resumo

A Silicon Ball (Si-ball) é um detector baseado em semi-condutores desenvolvido e construído nas instalações do ISOLDE-CERN, onde foi explorado por mais de uma década para investigar experimentalmente propriedades estáticas e dinâmicas de núcleos exóticos que são produzidos por meio da técnica ISOL. Devido a algumas limitações técnicas da época, o detector foi transferido para o *Centro de Micro Análise de Materiais* (CMAM) em Madrid, Espanha.

CMAM é um laboratório multidisciplinar, no qual diferentes feixes de iões de núcleos estáveis são hoje produzidos com um acelerador do tipo Tandem de 5 MV em combinação com duas fontes de iões diferentes. Tradicionalmente, uma das linhas deste laboratório de pesquisa foi dedicada à física nuclear fundamental, onde recentemente foram medidas reações a baixa energia relevantes para a astrofísica nuclear.

O objetivo da minha tese de Mestrado é a adaptação e o funcionamento da Si-ball como detector de partículas implementada recentementena na linha de física nuclear do CMAM, preparando-a para futuras campanhas experimentais dedicadas para investigar uma variedade de aspectos sobre a estrutura e dinâmica do núcleo atómico.

Durante a minha estadia em Madrid, trabalhei num quadro de colaboração que tornou possível a interação com pessoal científico e técnico experiente. O trabalho implicou desenvolvimentos ao nível da instrumentação electrónica e a realização de experiências que visaram o estudo e caracterização da resposta de detectores de *Silício* e da sua cadeia electrónica. O estudo passou pelo reconhecimento de vários componentes electrónicos integrados, dos softwares de aquisição de dados, software de programação e tratamento de dados, assim como a sua análise. Foram também abordados aspectos de tecnologia de vácuo, sistemas de diagnóstico de feixe em aceleradores de partículas e em particular detectores de estado sólidos com alta granularidade. A principal tarefa em que estive envolvido foi a calibração em energia dos detectores de Silício que compõem a Si-ball, utilizando vários tipos de fontes radioactivas emissoras de partículas α e determinando o valor da espessura da camada morta em cada um dos detectores funcionais que constituem a Si-ball.

Contents

List of Figures

List of Tables

Chapter 1

Introduction

Silicon, the element that revolutionized the development of electronics, is known as an important and multi-usable material, dominating today's electronic technology. Silicon is used in solar cells, computers and telecommunication systems. Originally Silicon comes from the Latin word *Silex*, *Silicis*, meaning flint. Over the past decades, Silicon has been implemented in charged particle detector systems, allowing for the discovery of new particles (like exotic nuclei) and the better characterization of the known ones. One of these detector systems is the so called Silicon Ball, from know on Si-ball [1], which was specially developed to originally encounter the nuclear physics researchers needs at the radioactive ion beam facility ISOLDE, CERN. This document presents an overview on the various hardware and software components related to the Si-ball detector, together with the study done on the characterization of the thickness of the dead-layer of the presently available units of the detector. To better know the working process of Silicon detectors we will also introduce some physics properties of microscopic behaviour of the atom.

1.1 Atomic nucleus and nuclear reactions

The universe is all that physically exists, the totality of space and time and all forms of matter, including all planets, stars, galaxies and the components of intergalactic space. But when we try to understand a little more about it we turn to the microscopic, the atom. Its center, the nucleus, gathers all the positive charge of the atom, and almost the totality of the atomic mass, with dimensions the order of femtometres (1 fm = 10^{-15}m). On the other hand, the electrons, negatively charged, orbit around the nucleus at very large distances of about 10^{-10}m, where the distance determines the atomic dimensions. The nucleus consists of A nucleons (Z protons and N neutrons) held together by the

strong nuclear force, a short range interaction which compensates the repulsion between the protons due to the Coulomb interaction.

Most of known nuclei are unstable and only some of specific configurations of protons and neutrons results in a particle-emission stable system. Presently 256 stable nuclides are known [2]. However, the nuclear landscape is dominated by unstable species. Through radioactive decays these systems of nucleons are transformed in others, till the stability is reached. Up to now around 3000 species which have been identified or characterized in laboratories worldwide [3].

To better identify all existing nuclides, they are represented in a bidimensional plot known as The Chart of Nuclei (fig. 1.1), where the horizontal and vertical axis represent the number of neutrons and protons, respectively. The limits of the region of stability against particle emission are defined by the drip lines. The drip lines are located in the frontier in which the separation energy for one proton S_p (for the left drip line or proton drip line) or one neutron S_n (right or neutron drip line) becomes negative. Exotic nuclei allow for the study of properties which are well established for stable nuclei and whose validity should be explored near the drip lines.

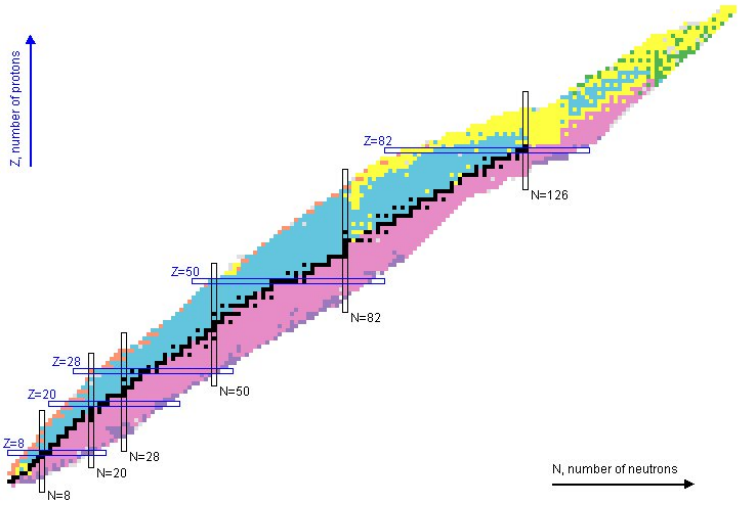

FIGURE 1.1: The chart of nuclei. Black squares represent the stable nuclides while the rest of isotopes are depicted in different colours, where each colour represents the most probable type of decay [4].

An important tool to explore the properties and production of exotic nuclei are nuclear reactions. When two particles collide, many different processes may occur with resultant energy part of it. The energy released during the reaction, Q, can be calculated as the the difference between the masses of the system before and after and also the kinetic energy of the particles after the reaction (E_f) minus the energy before the reaction (E_i). The Q value can be positive (exothermic reaction), negative (endothermic) or zero. There are different types of possible reactions:

- *Elastic scattering.* There are no internal changes produced and the Q-value of the reaction is zero (the observed particle is equal to the projectile, and the residual nucleus is the same as the target).
- *Inelastic scattering.* The residual nucleus after the reaction is left in a excited state, consequently Q = -E, where E is the energy needed to excite the particles.
- *Transfer reactions.* During this type of reaction, an exchange of nucleons between the target and the projectile occurs.
- *Capture reactions.* The target and the projectile form a system generally in an excited state, which subsequently decays by emitting one ore more gamma rays.
- *Fusion-evaporation reactions.* The target and projectile fuse in a compound nucleus which decays by emitting particles as well as gamma rays.
- *Breakup reactions.* The projectile, generally weakly bound, is broken into two or more fragments due to the electromagnetic (Coulomb breakup) and nuclear (nuclear breakup) field created by the target nucleus.

Nuclear reactions were and still are the tool to produce other nuclei whose properties can be studied, eventually again through nuclear reactions.

The next section explains the designation of exotic nuclei and the methods considered for its production.

1.2 Exotic nuclei

Coming back to radioactive nuclei, during their production in nuclear reactions many different species are usually formed and consequently, a method to select the nucleus of interest is needed. In general, for the production of exotic beams, two complementary methods are used, namely the Isotopic Separation On-Line (ISOL) and the In-Flight Separation (IFS) technique [5].

In an ISOL facility, a primary light beam (low mass) is produced from a driver accelerator which focuses on a thick target (in order of mm), producing the nuclei of interest that are diffuses into the ion source and off the target. Through the source, the different ions are extracted. To select the desired type of beam is necessary to carry out a mass separation using for this purpose their mass-to-charge ratio. Made the selection of the ions of interest these are accelerated. The main advantage of the ISOL technique is the high yield of radioactive nuclei produced, which is a consequence of the

use of thick targets and light ion beams as primary beams, as they can be produced with high intensities. However, this technique is limited by the so-called release time or time passed between the moment in which the radioactive species are produced and the moment of their extraction from the source, which is dominated by the diffusion time of the radioactive ions through the thick target. This result requires that only species with a long half-life of the order of milliseconds or more can be effectively generated and then accelerated at ISOL facilities.

In the In-Flight method, the primary heavy ion beam impinges on a thin light/low mass target producing radioactive nuclei by fragmentation or fission. The kinetic energy originating from the reaction products, already ionized, is of the same order of magnitude of the primary beam and thus enough to escape from the target. However, the reaction fragments are produced with a large spread pulse. These fragments then enter in a fragment separator (analysing magnet), where a particular isotope is selected according to both momentum and charge-to-mass ratio. The energy after the separator is usually high enough and no post-acceleration is needed [6], even though, it depends on the experiment. Unlike the ISOL technique, this method allows for the study of very short lived nuclei.

The study of exotic nuclei has shown increasingly interest over the past decades, due to their large N/Z ratios and impressive properties such as halo and skin. It is also important for other fields like nuclear astrophysics, the properties of exotic nuclei are utmost essential to understand the nucleosynthesis in the r process. From theoretical prepositions, new exciting discoveries had been made experimentally. For example, a new phenomenon, the nuclear halo, a state in which nucleons spread like a thin mist around the nucleus, was first discovered in ^{11}Li in 1985 [5, 7], and later in many other light exotic nuclei as well. Since then more and more exotic nuclei have been investigated with various modern experimental methods to better understand this curious phenomenon. For nuclei far from the beta(β)-stability valley and with small nucleon separation energies, the valence nucleons extend over quite a wide space to form low density nuclear matter, i.e. a nuclear halo. Furthermore, the Fermi surface for exotic nuclei is usually very close to the continuum threshold. The valence nucleons could be easily scattered to the continuum states due to the pairing correlation. Thus, theories which can properly handle the pairing and continuum states are needed to describe the properties of exotic nuclei [5].

Exotic nuclei show other interesting phenomena such as the disappearance of traditional shell gaps and the occurrence of new ones, which result in new magic numbers. The current nuclear models are mainly based on the knowledge obtained from the nuclei near the β-stability line. For instances, the cornerstones for the edifice of modern nuclear

physics include shell model and collective model, which are respectively based on the magic numbers (the stability of some nuclei compared with their neighbours) and the incompressibility of the nuclear matter. Therefore the change of magic numbers and the unprecedented low density nuclear matter in halo nuclei have shaken the foundation of nuclear physics. New innovative nuclear models are needed to describe the exotic nuclei characterized by weakly binding and low density [5].

This concern on the study of exotic nuclei and all the theory behind motivated the upgrade of the resources that are able to produce these exotic systems. Nowadays nuclear physics is entering in a new era for particle detection as many Radioactive Ion Beam (RIB) facilities are operative, or in some cases being upgraded, under construction or planning to be constructed, as shown on fig. 1.2. Among the ISOL facilities we count the ISOLDE CERN in Switzerland and its upgrade HIE-ISOLDE, GANIL in France which will soon welcome the SPIRAL2 facility, or the TRIUMF laboratory in Canada. Regarding fragmentation facilities, we list the HIRFL in China, RIBF in Japan, GSI and its upgrade FAIR in Germany, or the NSCL facility and the upcoming FRIB in the US. These new facilities together with developments in the detection techniques have changed the nuclear physics scenario, making it possible to produce and study nuclei far away from the stability line.

FIGURE 1.2: Representative distribution of present and projected major facilities for rare-isotope beams [8].

Besides the panoply of facilities operating, there must be a goal behind the experimental studies, and it is where the theory appears to reinforce the study of exotic nuclei.

The RMF (Relativistic Mean Field) is one of the best candidates for the description of exotic nuclei. In order to describe exotic nuclei, the pairing correlation and the coupling to continuum, which are extremely crucial for the description of drip line nuclei, must be taken into account properly [9].

The next section provides a quick overview on the studies performed over the past decades on exotic nuclei, concentrating on experiments done detecting charge particles.

1.3 Nuclear physics studies using charged particle detectors

The theory behind exotic nuclei is established on strong studies made all over the past 50 years [5, 10]. To understand the world around us and to comprehend how the Universe developed to where it is today we must study the atomic nucleus and how a complex many body system behaves. It's a fundamental needed to understand how such a system can be constructed and its decay be described, from what we know at present for its nuclear constitution, protons and neutrons, interacting through well known forces. The nucleus is a complex many particle system in which the residual interactions of various types may lead to collective excitations which can have a strong effect on the β-decay properties [10]. In nuclear physics, β-decay is a type of radioactive decay in which a proton is transformed into a neutron, or vice versa, inside an atomic nucleus. This process allows the atom approach to the optimum proton-to-neutron ratio. As a result of this transformation, the nucleus emits a detectable β particle, which is an electron or positron [10]. β decay is mediated by the weak force. There are two types of beta decay, known as beta minus and beta plus.

β^+ decay is thus also known as positron emission. The strength in the daughter nucleus of β decay distribution determines fundamental nuclear properties as the half-life, the rate for β-delayed particle emission and the shape of the emitted electron/positron and (anti-)neutrino spectrum [11].

The study of exotic nuclei can help to isolate and amplify specific aspects of nucleonic interactions due to their asymmetric neutron-proton balance, reaching the limits of nuclear binding, the so called drip lines.

These lines (shown in fig. 1.3) have uncertain limits and they are only known experimentally for light nuclei. The proton drip-line is closest to the β-stability line since the Coulomb repulsion prevents nuclei with very large proton excess from being bound.

For the study of drip line nuclides, different experiments are usually performed in order to obtain as much information as possible, information that has to be properly combined to extract relevant nuclear properties. Due to the low intensities achievable with radioactive beams in comparison to stable beams, a remarkable effort has been made in order to develop new experimental techniques. Experiments have been targeted to measure elastic scattering, spin and momenta or nuclear states, nuclear masses, β decay and β-delayed particles emission, fusion, correlations, momentum distributions, reaction cross sections [5].

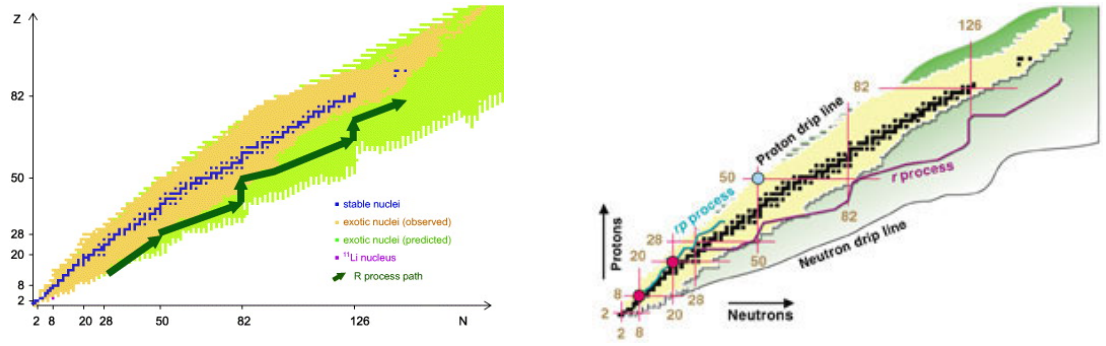

(a) (b)

FIGURE 1.3: Exotic Nuclei Map. The figure (a) shows the different nuclides present in nuclei map in relevant importance to stable nuclei and exotic nuclei. The figure (b) shows the proton and neutron drip lines in more detail situated.

The experiments carried out in order to study elastic scattering and obtain interaction and reaction cross sections provide information about nuclear size and density distributions [5, 10]. These are important properties used in order to establish nuclear potentials or single particle configurations.

The primary map region of one proton radioactivity is located between Z=50 and 82, and it turns out that a considerable number of nuclei exhibit this decay mode either from the ground state or from an isometric state or both [5, 10]. This information permits to map the drip lines of the region while testing the validity of the single-particle picture far from stability.

The studies for which the application of Si-ball serves the best are multiple decay modes (β-p, β-2p, β-α, β-pα) that are energetically open and occur more frequently from excited states and for exotic systems with a lower Z [5]. These β-delayed particle studies were fundamental on helping to understand the new nuclei. In addition the 2 proton emitters are the new age of β-delayed particle studies [5].

The first β-delayed proton precursor, ^{25}Si, was studied thanks to the use of Si surface-barrier detectors, the first application of this device in Nuclear Physics. But it was also studied by other groups and reviewed in 1966 [1], with ten β-delayed proton precursors known at the time. A review of β-delayed proton and α emission with over seventy eight precursors and their branching ratios were publisehd in volume III "Particle emission from Nuclei" [1]. Today 160 precursors ranging from ^{8}B to ^{183}Hg are known.

More recently the work developed at ISOLDE (CERN) with Si-ball on β-decay was substantially focused on β-delayed multi-particle decays [1]. And in general the Si-ball is an excellent position sensitive device with good granularity, efficiency and particle discrimination. The β-2p decays had special attention in the case of ^{31}Ar and for ^{22}Al the

distinction between β-p, β-2p and β-α branches was possible with the Si-ball detector [1]. Other important case is the exotic decay channels that are predicted to occur from highly excited sates in nuclei at the neutron drip line, as it happens in the light di-neutron halo nucleus ^{11} [1, 7]. It is of utmost importance because the complexity of the decay with many different open multi-particle channel and the understanding of the nuclear halo properties. Other application of the detector array is an expressive accuracy to measure β-delayed protons and the study of isospin symmetry via Gammow-Teller decays [1]. As study $^{58}\text{Zn} -> {}^{58}\text{Cu}$ decay was considered. Other investigations made at ISOLDE included electron-neutrino correlations in Fermi decays for ^{32}Ar, and the search for proton decay from the ground state in astrophysically relevant nuclei, as ^{69}Br or ^{74}Rb [1].

Other applications considered with Si-ball were the study of the α-decay of ^{12}B [1]. States located above the 3-α threshold in ^{12}C are crucial to understand the triple-α process in red giants. This process is enhanced via the 7.65 MeV 0^+ state, and the 2^+ state located above it. Nevertheless the exact position of this 2^+ state is not known and the spin, width and position of the broad 10.3 MeV state, and its interference with the 7.65 MeV state, are still uncertain. The nucleus ^{12}C can be populated at ISOLDE via the β-decay of ^{12}B [1]. The simultaneous detection of α particles and the discrimination from β particles with the ISOLDE Si-ball in combination with Double Sided Si Strip Detectors, provided important information on its excited structure.

To perform these studies a parallel development of modern production facilities RIB's (such as HIE-ISOLDE, already operational) and efficient detection systems as Si-ball is needed. The two main facilities in which the Si-ball detector was used will be discussed in Chapter 2. The Si-ball detector, which will presented in Chapter 3, offers optimal performance also to carry out systematic studies of nuclear reactions between stable nuclei allowing for high precision measurements of elastic scattering, angular distributions and the determination of optical potentials.

Chapter 2

Particle accelerator facilities

The study of those "new" particles can be real only with the proper infrastructures. Presently there are several facilities which provides very sustainable and optimized conditions to prepare and execute many of these experiments. They are not only able to manage several experiments but also to provide an multi-international acknowledgement of the various researchers and countries involved with their contribution, as mentioned in section 2.1. This chapter also reference the ISOL-type facility where the Si-ball was developed, section 2.2. These facilities are also considered as an important bridge between the theoretical and the experimental investigation, which became the most significant aspect to study the atomic nuclei. One of those facilities is CMAM, described on section 2.3, where the Si-ball are presently operating.

2.1 Role of particle accelerators in nuclear physics

Particle accelerators are devices used in nuclear physics to accelerate ions produced in an ion source with little energy (tenths of keV) and accelerated to a kinetic energy ranging from 1 MeV up to hundreds. Accelerators are required to characterized systems as small as atomic nuclei ($\sim 10^{-15}$ m) in studies of its structure and the forces that act on it via nuclear reactions in many cases [12].

In nuclear reactions when the kinetic energy obtained from the acceleration stage is sufficiently high, the produced nuclear collisions, overcome the Colombian repulsion in the positively charged nuclei, and effects of the nuclear force occur. Nowadays a wide range of particle accelerators exist such as tandem, Van de Graaff, cyclotron, etc... Typically, tandem type accelerators have two phases. In the first phase a beam of negative ions is injected from an ion source through the terminal at zero potential and is

accelerated to the positive terminal in the middle of the tandem vessel, which contains a stripper made of a gas (typically N_2) or a thin carbon foil. In the stripper, ions lose electrons reaching a positive charge state that makes them to be accelerated away from the positive terminal. The difference species of ions exiting from the tandem are subsequently separated by magnets and directed to the reaction target [13].

2.2 ISOLDE-CERN facility

CERN (*Conseil Europeen pour le Recherche Nucleaire*, Switzerland) is one of the largest research facilities in world. It was founded in 1954 as a European project involving 12 countries and is placed in the border between France and Switzerland. These members (in alphabetical order) were: Belgium, Denmark, France, Germany, Greece, Italy, Netherlands, Norway, United Kigdom, Sweden, Switzerland and Yugoslavia. Currently, the participating countries amounts to 22 in addition to the founders, which are: Austria, Bulgaria, Czech Republic, Slovakia Republic, Spain, Finland, Hungary, Poland and Portugal.

The main lines of research focus on fundamental physics, following out the purpose for which CERN was built: understanding the universe and how it works. To do this, CERN has several accelerators and numerous complex detectors [14]. But CERN is not only a place of research, it is also the banner for international collaboration in research, a place where researchers from diverse disciplines and backgrounds exchange knowledge and open their careers to new contacts and new technologies and where tomorrow's future researchers give their first steps in science.

Most of the work carried out at CERN it is possible due to different accelerator rings that are present in this facility. In fig. 2.1 accelerators scheme and some of the facilities at the laboratory can be seen. The first stage of a proton along throttle systems occurs in the linear accelerator Linac2, which are injected after being obtained by the ionization of hydrogen in Duo Plasmatron ion source. After being initially accelerated, the protons pass to the PSB (Proton Synchrotron Booster) and from there they are injected into the PS (Proton Synchrotron). The protons can be directed to different CERN facilities or may remain accelerated for higher energies. This way, protons which are leaving the PS can enter the SPS (Super Proton Synchrotron) and then to the newly opened LHC (Large Hadron Collider), but also are guided to ISOLDE where are produced radioactive ion beams [15].

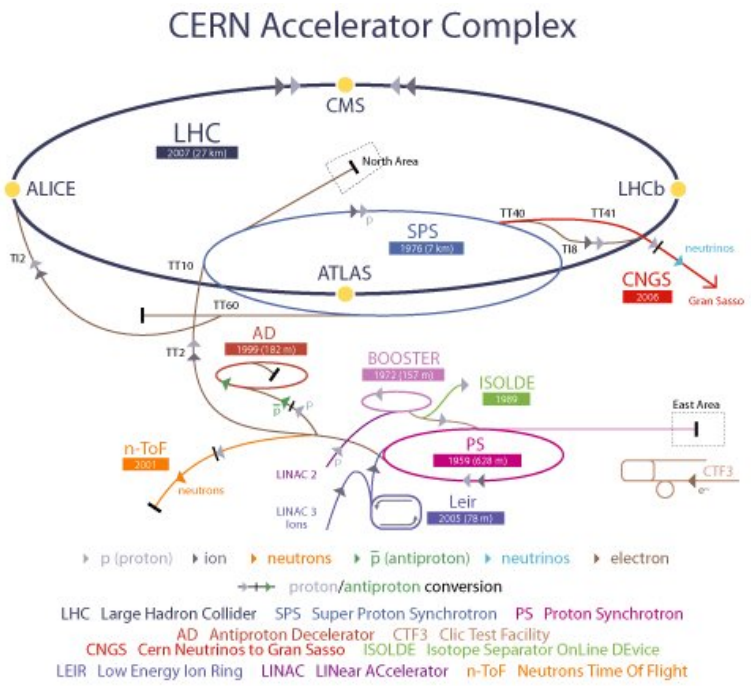

FIGURE 2.1: Schematic view of existing accelerators and beam lines at CERN [15].

ISOLDE

ISOLDE (Online Isotope Mass Separator) is a facility dedicated to the production of a large variety of radioactive ion beams for many different experiments in the fields of nuclear and atomic physics, solid-state physics, materials science and life sciences. It began in 1964 as an experiment in a group denominated radio-chemical who used the synchrotron to produce beams in exotic radioactive reactions. Since then, it has undergone several improvements. The facility is located at the Proton-Synchrotron Booster [16].

There are several research lines at ISOLDE (see fig. 2.2). Because of the high variety of chemical species that can be created it makes possible to study systematically atomic and nuclear properties and exotic decay modes away from valley of stability, allowing us a better understanding of the atom (with implications in other fields like astrophysics). The possibility of performing implantations of radioactive species in pure materials enables research in solid state physics, in particular in the study of defects and impurities in semiconductors. In addition, it is possible to conduct studies on diagnostics and therapy with radioactive isotopes. Radioactive beam production is performed through the ISOL (Isotope Separation On-Line) method specialized on a thick white at high temperature. The ISOL method consists in producing a secondary ion beam by means of a primary beam (usually protons) impinging on a thin target, which produces species which are accelerated. The main advantage is that the beams side produced are generally more intense (high emittance) than those produced by the fragmentation method (due to its

thicker target). The ISOL method provides beams of relative low energy, so another method must used when energies of hundreds of MeV are required.

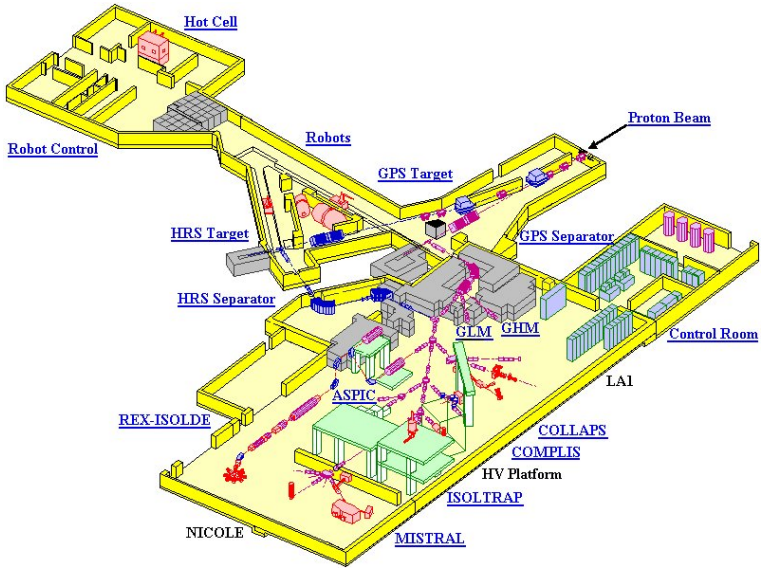

FIGURE 2.2: Schematic of accelerators and beam lines at ISOLDE-CERN [15].

Because of the strong links between the scientific communities at CMAM and at ISOLDE, the detector Silicon Ball, developed at ISOLDE, was recently transferred to the CMAM facility in Madrid, Spain. The following section describes the laboratory and the specific beam line in which the detector has been installed.

2.3 CMAM

The CMAM (*Centro de Micro-Análisis de Materiales*, Madrid, Spain) is a research center belonging to the UAM (*Universidad Autónoma de Madrid*), which operates an electrostatic ion accelerator of tandem type with a maximum terminal voltage of 5 MV, dedicated to material analysis, modification of materials and to the study of nuclear reactions with stable nuclei at low energies. The equipment present at CMAM results on multiple lines. At the end of the accelerator there are attached different beam lines dedicated to different areas of application, as well as for fundamental studies and auxiliary equipment (micro-analysis techniques, sample preparation, ...) [13].

2.3.1 The Tandem accelerator at CMAM

Presently in CMAM there is one of Tandem accelerator (see a sketch in fig 2.3).

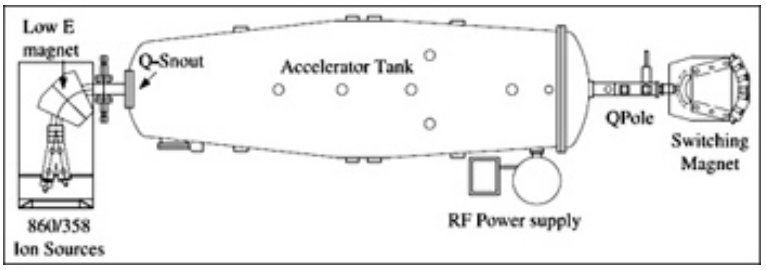

FIGURE 2.3: Tandem accelerator at CMAM-UAM with ion sources to select the beam isotope to be accelerated [13].

Ion sources

In CMAM there are two ion sources that can efficiently ionize any stable isotopes from hydrogen to uranium:

- Duoplasmatron source
- Sputter ion source

The Duoplasmatron source (model HVEE-358) is a gas source mainly functioning for producing He and H. In the Model 358 Duoplasmatron, a two-stage discharge is integrated in the generation of the ion beam. The first discharge is sustained by the thermionic electron emission from a filament (cathode). An intermediate electrode acts as the anode for the first discharge and is equipped with an aperture in its center. The discharge is guided through the axial magnetic field in the aperture into the second discharge chamber. The second discharge is maintained between the intermediate electrode, which now acts as a cathode, and the main anode. The strong axial magnetic field generated in this region, confines the plasma into a small volume, and is responsible for the high plasma density. The ions from the second discharge flow through the anode aperture into the extraction region.

The Duoplasmatron source can be configured to produce both, negative and positive ions. H^- can be directly obtained from the source, with currents of few tens of microamps. However, the process is not so efficient for producing He^-. Then, the source is operated in "positive mode", i.e. He^+ ions are produced. After being extracted from the source, He^+ ions are injected into a Lithium charge-exchange channel. Inside this channel, Li vapour exchange electrons with He beam, becoming this negative. Duoplasmatron source produces typically hundreds of microamps of He^+. The efficiency of Lithium canal is around 2% giving as a result a few microamps of He^- at the entrance of the accelerator.

The negative sputter ion source (model HVEE-860) is able to produce negative ion beams from solid sputtered targets. The ions are produced by bombardment of the

target with Caesium ions, which is covered also with a Cesium thin layer as a result of condensation of the vapour onto the cooled target surface. The sputtered atoms interchange electrons with Cs when they pass trough this layer, becoming negative ions. Since negative ions are produced directly, it's not necessary to use an additional set-up like the Li-channel. The negative ions are then repelled towards the extraction region, while the secondary electrons produced in collisions are eliminated from the negative beam by means of a permanent magnetic field.

For certain species (e.g. Nitrogen), it is not possible to obtain negative ions, due to its negative electron affinity. Then, a molecular beam (e.g. NH^-) is created, injected and accelerated until the terminal electrode, where is broken thanks to collisions with the same gas used for stripping electrons. The positive ion (N+ in our example) is, then, normally accelerated in the second stage.

Tandem

One of the main equipment that are part of the center CMAM it is an electrostatic type tandem accelerator having a terminal with a maximum voltage of 5 MV. It was designed and manufactured by the company High Voltage Engineering European, the first coaxial tandem accelerator capable of achieving high current at 5 MV, using a voltage multiplier Cockcroft-Walton type. The ions are accelerated in two steps. The terminal with a voltage V_0 is at the center of the accelerator tube. In the first stage the negatively charged ions, charged q_1, accelerate up to the terminal acquiring a kinetic energy $q_1{*}V_0$. After this first step, the beam passes through the charge exchange region, denominated "stripping". Thus, the ions which it had negative charge q_1, become q_2 with positive charge. In the second step, the positive ions are accelerated from the positive voltage terminal to the end of the accelerator tube (ground), a similar process to the first step. The ion beam acquire a kinetic energy at the end of the tube which corresponds to the sum of the energies obtained in each step. Just off the accelerator tube is a first magnet switch, which redirects the beam to the beam line of interest [13].

Switching Magnets and Reaction lines

The installation of Tandem accelerator, which originally had a universal base line was developed to meet various operating areas in CMAM. Some extension lines shown in fig. 2.4, have been built and some are under development. Four lines are routinely available to users, offering a range of different techniques to analyse and modify materials, and perform basic studies in nuclear reactions:

1. The Standard multi-purpose line

2. The External Microbeam line

3. The ERDA-TOF line

4. The Nuclear physics line

5. The implantation line

6. The Internal Microbeam line

The users can rely on installations that, by the kind of beams and instruments available and their performances (e.g. space, time, angle, energy resolution, current, fluence, etc.) allow to deal with many research topics. These are like the production and characterisation of materials at the technological edge like materials for photonics and the electronic industry; the controlled implantation of ions to modify materials properties; the high sensitivity non destructive analysis of fine arts objects and environmental samples. Some other lines, now in development are ready to expand the range of materials and conditions that can be altered and/or analysed. The next lines to be available are in gray in fig. 2.4.

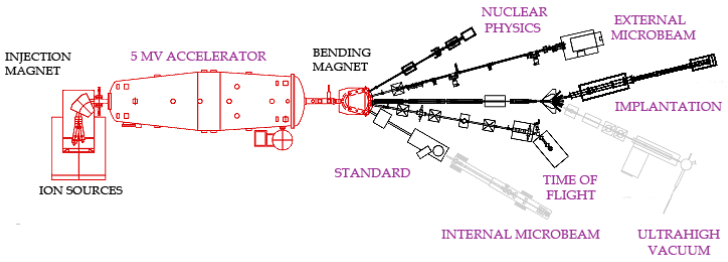

FIGURE 2.4: Schematic of Tandem accelerator and experimental lines at CMAM. The dark ones are already implemented and operational, while the grey are in construction [13].

The steps outlined in this thesis get special attention on test bench of Si-ball detector, located in Nuclear Physics line.

2.3.2 Nuclear physics line

The studies carried out in CMAM based on techniques of nuclear reactions come as a result of a collaboration between the IEM (*Instituto de Estructura de la Materia*) of the CSIC (*Consejo Superior de Investigaciones Científicas*) and UAM, which was launched on the Nuclear Physics line shown schematically in fig. 2.5. Nuclear Physics line is compatible with high vacuum conditions and is particularly designed to connect easily with the purpose of having a variety of experimental setups. This makes it one of the most versatile setup, being possible to carry out experiments and studies of nuclear

reactions, characterization detection systems, etc. The line is located at front of the accelerator at an angle of -30° and is equipped with two sets of slits for defining the beam shape and size. It is divided in two sections: **Section 1** Observation beam, where the ion beam is guided for the experimental line and includes the tools "beam profile monitor" which controls the beam current by measuring and a collimator where the use of "Faraday Cup" can control the beam enter in chamber or in the line; **Section 2** Experimental, where the beam clash on the target present in the chamber. This section is designed to be as flexible as possible to exchange experimental chambers, allowing the assembly to have a wide variety of teams working and detectors mounted, such as Si-ball, which is described in the following chapter.

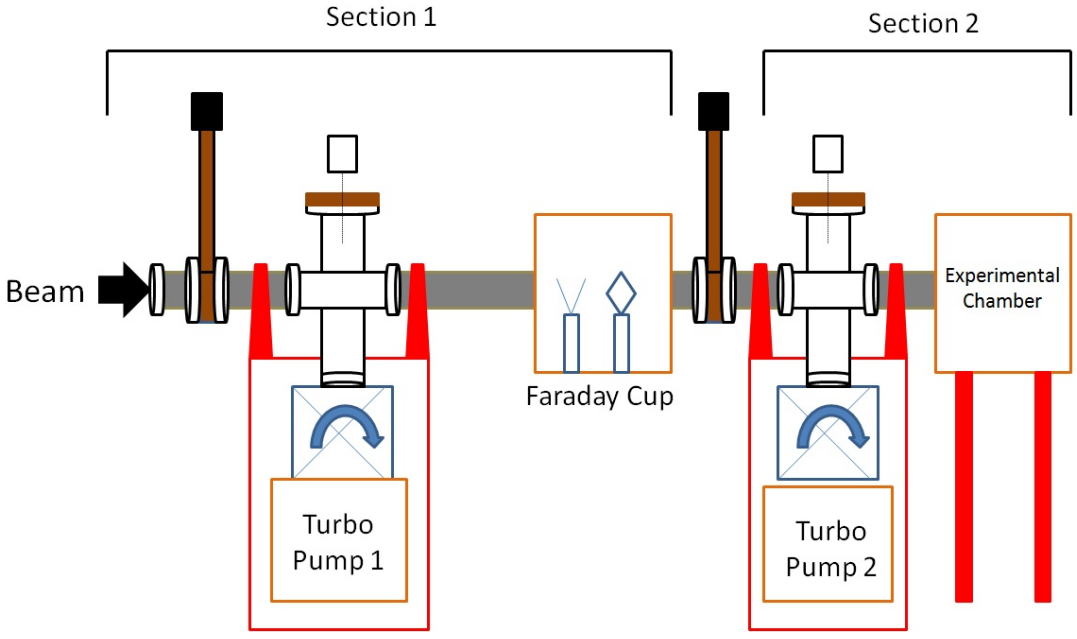

FIGURE 2.5: Schematic of physics line with the described vacuum pumps, Faraday cup and the reaction chamber at the end of the line [13].

2.3.3 Reaction chamber

At the end of the line we have the reaction chamber (fig. 2.6), which operates at different levels. Pressures of order of 10^{-6} mbar are usual in the acceleration line as well as in the reaction chamber. It is done by the vacuum system operating in the end of the beam line. It consists of two rough pumps and two molecular pumps. For security reasons and as mentioned before there are two sections, so each pump is designated for each section. Connected to the chamber there is also a cooling system that prevents the detection system to work at high temperatures which spoils its performances.

FIGURE 2.6: Reaction chamber at the end of nuclear physics line at CMAM, with multiple entries and designed for different apparatus [13].

The Si-ball has a specifically designed chamber which are now installed at the end of the nuclear physics line at CMAM laboratory. This chamber will be described in detail on next chapter and also the tools that make part of it.

Made the description of the entire infrastructure that will be the base of operation of the Si-ball and all the infrastructure where was previously designed and developed, we will pass to the fundamental description and the composition of Si-ball. In particular we talk about Silicon detectors that will be described in the following chapter.

Chapter 3

Si-ball detector

This chapter will retreat the Si-ball detector and its main components, introducing the main character of the work done in Master Thesis. The first subject to be addressed in section 3.1 will be the physics interests that motivated its construction as well as listing the first studies done with it. Followed by a general description of detection

3.1 Si-ball motivation and previous experiments

Recent advances in the production of beams with weakly bound nuclei, outside the nuclear stability valley, needs the development of spectroscopy devices with high intrinsic and geometrical efficiency and also its granularity. The track detector devices in study make good chances to get favourable results on unstable atomic nucleus which are being discovery at it most.

3.1.1 Motivation and requirements for Si-ball

As already mentioned in section 1.3, β decay is one of the most relevant nuclear processes that provides interesting information for the investigation of the nuclear structure of exotic nuclei. The detection of charged particles over a wide range of energies keeping a high energy resolution as well as a low energy threshold is mandatory when studying the β decay of exotic nuclei.

Related to the understanding of the nucleus via nuclear reactions, it is also necessary the detection and identification of the charged particles resulting from the reaction process, in addition to the determination of its kinetic energy and angular distribution.

Detection sensitivity and granularity are also for these cases requested when planning for the construction of a detector device to study these processes.

The Si-ball detector was build aiming at covering all these premises for the study of fundamental properties of exotic nuclei. As it will be shown throughout this chapter, it covers a large energy range (100 keV to 12 MeV) keeping a good energy resolution (1% at 5 MeV) and providing a high geometric and intrinsic efficiency for charged particle detection. Particle identification could be done as well combining techniques as pulse shape discrimination or Time of Flight [1].

After its construction, as it will be presented in the next section, first studies using Si-ball concentrated on the characterization of the β decay of exotic nuclei. However, due to its large angular coverage, high granularity and close to 4π geometric efficiency, it is a very suitable device for the study of angular distributions of charged particles resulting from nuclear reaction experiments, as they will be considered in the future at the CMAM tandem laboratory.

3.1.2 Previous experimental studies with Si-ball

As already mentioned, Si-ball was designed to cover large energy dynamic range keeping simultaneously a good energy and angular resolution. Under these premises, it already allowed the execution of several experiments at the ISOLDE CERN facility. Here we list the most relevant studies in which the Silicon Ball can show its capabilities and some already performed at this facility:

- β-delayed particle emission in ^{31}Ar [17] and ^{22}Al [17].
- Ground state proton decay in ^{69}Br [18] and ^{73}Rb [18] relevant for nuclear astrophysics.
- β decay from highly excited states in the halo nucleus ^{11}Li [19].
- Electron-neutrino correlations in Fermi decay from the nucleus ^{32}Ar [1].
- β disintegration in ^{17}Ne [14] and ^{33}Ar [14].

Besides its motivation and the already performed studies, in order to fully understand the principles behind Si-ball the following sections will present some basic concepts regarding the characteristics of radiation detectors.

3.2 General characteristics of detectors in nuclear physics

In general, nuclear radiation detectors present on a general view similar principal of characteristics, such as a specific window through which particles reach the detector, a certain kind of interaction with the radiation or the release of a large number of low-energy electrons from the atoms in the detector material. These released electrons are collected and grouped into a voltage or a current pulse for analysis by an electronic circuit. For this analysis the choice of material to detect the radiation it's important to gather the information which we are trying to get [11].

For α particles originating from radioactive decays or charged particles from nuclear reactions, at low energies (few MeV), very thin detectors with maximum thickness of 100 μm are sufficient. For electrons emitted in β decay the thickness necessary is in a range between 0.1 to 1 mm, a type of detector for which the proportionality of the energy of the particle to the generated output is warranted.

In order to characterize the energy of a certain kind of radiation we should choose a type of a detector for which the proportionality of the energy of the particle to be generated output signal is warranted. In addition we must choose a material for which the number of released electrons is sufficiently large to achieve the desire energy resolution. Complementary if we want to determine the time properties of the emitted radiation, we must choose a material for which the electrons can be gathered quickly into the pulse. If we are willing to measure at a high count rate the detector should be able to recover quickly before the next particle arrives. On other hand, when aiming at low counting rates we should be to detect every single event and reduce the influence of background radiations. Also if we would like to perform tracking of particle trajectories we should have a detector sensitive to the position at which the radiation enters the detector.

Nuclear and elementary particle physics are based on the development of many different types of detectors. However are all based on the same fundamental principle, the transfer of part or all of the radiation energy to the detector mass where it is converted into some other form, usually an electric response. Charged particles transfer their energy to matter through direct collisions with the atomic electrons, exciting or ionizing electrons in material. The form in which the converted energy appears depends on the detector and material design. Nowadays modern detectors response are of electrical nature. The information from the detector is transformed into electrical impulses created by electronic means. The great progress in electronics and computers to provide a faster and more accurate treatment of the information also contributes to the effective use of the systems. In the following the general characteristics relevant to a radiation detector will be depicted.

Sensitivity

The primary consideration for a detector is its sensitivity, i.e. the capability of producing a usable signal for a given type of radiation and energy. Any detector is sensitive to all kind of radiation or energies, however, as their response is not homogeneous, they are designed to be sensitive to certain types of radiation within a given energy range. If the energy is outside of this region it usually results in an useless signal or in a greatly decreased efficiency. The sensitivity of a detector is characterized by the following factors: the cross section for ionizing reactions in the detector material; the detector mass; the inherent detector noise and the protective material surrounding the sensitive volume of the detector, the so called dead-layer.

The detector mass and the cross section for ionizing reactions set the probability of an incident radiation to convert part or all of its energy in the detector.Considering the particular case of detecting charged particles, as they are highly ionizing, most detectors, even of low density and small volume, will have some ionization produced in their sensitive volume. On the contrary, for neutral particles this interaction cross section is usually much smaller so that a higher mass density and volume are necessary to warranty a reasonable interaction rate, otherwise the detector becomes transparent to the radiation. A lower limit from the minimum amount of signal produced in the detector via ionization is determined by the noise from the detector and from the associated electronics, The noise appears as a fluctuating voltage or current (common on all electronic devices) at the detector output and is always present whether there is a signal (radiation) or not.

Another limiting factor for the sensitivity of a detector is the material covering the entrance window of the sensitive volume of the detector, the so called dead-layer. Because of the absorption in this layer, only radiation with sufficient energy to penetrate this layer can be detected. The thickness of this material thus sets a lower limit on the energy that can be detected.

Detector response

Other function in detectors is the capability of providing some information on the energy of the radiation. The amount of ionization produced by radiation in a detector is proportional to the energy lost in the sensitive volume. If the detector is sufficiently large, to completely absorb the radiation, this ionization gives a measure of the energy of the radiation.

Commonly the output signal of electrical detectors is in the form of a current or voltage pulse. The total ionization collected is reflected in the electrical charge contained in this signal, i.e., the integral of the pulse representing time. Considering that the shape

of the pulse does not change from one event to another, it is known the integral is directly proportional to the amplitude or pulse height of the signal. The response of a detector corresponds to the relation between the total radiation energy collected and the total charge (pulse height) of the output signal.

For many detectors the response is linear, or approximately linear, in a certain range of energies. In general the response on the particle type and energy and we can not assume that the linear response for one type of radiation will be linear for another. The characteristic of this response will be discussed later.

Energy resolution

The principle task in a most detector system is the detection of the energy of the radiation and the consequent transmission of the signal. Thus, the energy resolution is one of the most important factor of the detector characteristics. It is very important to know how close the signal can be and the detector can still resolve them. In general the resolution can be measured by sending a mono-energetic beam of radiation into the detector and analysing the resulting spectrum. Ideally we would obtain a sharp delta function peak, but due to fluctuations in the number of ionizations and excitations produced we usually observe a peak structure with a finite, width most likely of a Gaussian shape. Normally the resolution is given in terms of the full width at half maximum of the peak (FWHM). Energy signal which are closer than this interval are usually considered unresolvable. In general, the resolution is a function of energy deposited in the detector with the ratio improving ($Resolution = \frac{\triangle E}{E}$). It's assumed to be a contribution from Poisson statistics of ionization and excitation. It means that the average energy required to produce ionization is a fixed number dependent on the material. Thus as energy increases, the number of the ionization events also increases, resulting in smaller relative fluctuations and the consequent energy resolution improvement.

The response function

The response function of a detector at a given energy is determined by the different interactions which the radiation can undergo in the detector and its design and geometry [20]. As an example we can think on a monoenergetic charged particles, electrons for example, impinging on a detector thick enough to stop them. If we know that these electrons lose their energy in atomic collisions, the layout spectrum is predicted to be a Gaussian peak. But is predictable that some of these electrons will scatter out of the detector before fully depositing their energy, what produce a low energy tail. And other electrons can emit bremsstrahlung photons which may escape from the detector, providing again some events at a lower energy than the peak. So the final "product", the response of the detector to the detected particles, is a Gaussian peak with a tail

originated by the scattering and bremsstrahlung energy losses. However the response function could be improved once more by changing the geometry and design of the detector. Also the lower atomic the number Z, the lower the effects due to backscattering and bremsstrahlung.

Efficiency

The absolute or total efficiency of a detector is defined as that fraction of events emitted by the source which is actually registered by the detector. The absolute efficiency is also the result of the product of two efficiency factors: the geometrical efficiency and the intrinsic detection efficiency. The intrinsic efficiency is known as the fraction of events actually hitting the detector which are correctly measured. This probability depends on the interaction cross sections of the incident radiation in the detector medium. The intrinsic efficiency thus varies with the type of radiation, its energy and the detector material. In general, the intrinsic efficiency for charged particles is high for most detectors because of the easily ionization produced from a charged particle. Despite of that, heavy particles quenching effects are present in some materials draining the ionization produced. The geometrical efficiency corresponds to the ratio between the solid angle covered by the detector to the total solid angle in which the particles are emitted.

Response time and dead time

The response time of a detector is a very important characteristic, and it represents the time which the detector takes to form the signal after the arrival of the radiation. Its significant for the detector characteristics that the signal arrives quickly formed into a sharp pulse with rising flank as close to vertical as possible. In this way a more precise moment in time is marked by the signal. Its duration is also important because during the period in which the signal is been read no other event can be detected nor analysed, this happens because the detector is insensitive or because the second signal will overlap on the first. This contributes to the dead time of the detector and limits the count rate at which it can be operated [20]. These losses affects the observed count rates and distort the time distribution between the arrival of events. When we calculate the effects of the dead time, the whole detection system must be taken into account, as every electronic component of detector system has its own dead time.

These properties are as well applicable to Silicon detectors like the ones implemented in Si-ball. But in order to fully understand how these system works, the next section will present in more detail the principles that govern the interaction of radiation with matter, in particular with Silicon.

3.3 Silicon detectors properties and proton and heavy ions detection

The physical properties of silicon are in essential described as a hard, dark-grey solid with a bluish tinge. For common temperatures, Silicon is inscrutable to air. At high temperatures, silicon reacts with oxygen, forming an inert layer of silica. In nature it is found in the form of silicon dioxide and complex silicates. Silicon is the seventh most abundant element in the universe and the second most abundant element in the earth's crust. Today, Silicon is produced by heating sand (SiO_2) with carbon to temperatures approaching 2200°C. The discovery of Silicon was attributed to Jöns Jacob Berzelius in 1824, a Swedish chemist,by heating chips of potassium in a silica container and then carefully washing away the residual by-products. Silicon is a semiconductor and a solid matter, which isolates at low temperatures and shows a measurable conductance at higher temperatures. The specific conductance of 10^2 to 10^{-9} $\Omega^{-1}cm^{-1}$ lies somewhere between metals and insulators.

Since the development of quantum mechanics the electrical conductance can be explained with the covalent bond in the crystal lattice. Bound electrons can be excited by inducing energy above threshold energy (gap energy), e.g. energy from light, x-ray or β -particles. Since the 1960s semiconductors have been used as particle detectors. Initially, they were operated in fixedtarget experiments as calorimeters and as detectors with a high-precision track reconstruction. Since the late 1980s they have been widely used in collider experiments as Silicon microstrip or Silicon pixel detectors near the primary vertex. Silicon sensors have a very good intrinsic energy resolution: for every 3.6 eV released by a particle crossing the medium, one electron-hole pair is produced. Compared to about 30 eV required to ionize a gas molecule in a gaseous detector, one gets 10 times the number of particles in Silicon. The average energy loss and high ionized particle number with 390 eV/μm$\sim$108 (electron-hole pairs)/μm is effectively high due to the high density of Silicon. The usefulness and success of Silicon can be explained in a handful of keywords: existence in abundance; energy band gap; possibility to change gap properties by defined adding of certain impurity atoms (dopants) and the existence of a natural oxide.

3.3.1 Semiconductor detectors

Semiconductor detectors are based on crystalline materials predominantly composed by Silicon or Germanium. The real development of these materials took placed in the late 1950's, although their significant jump to commercial purposes only took place in the

1960's [21]. These devices can provide high resolution for energy measurements and are adopted in various areas of physics including nuclear physics, where are used for charge particle detection and gamma spectroscopy.

Germanium and Silicon are the most common and form the solid crystals in which the 4 valence atoms form four covalent bonds with neighbouring atoms. All valence electrons thus enter in covalent bonds, and the band structure shows a filled valence band and a empty conduction band [11]. To have a comparison the gap energy difference for an insulator is 5 eV and for a semiconductor is 1 eV. When the electrons are thermally excited they cross the gap into the conduction band, leaving a free space in the valence band known as hole. As an electron from a neighbouring atom fills the space, creating a new hole, a migration by the hole through the crystal seems to appear.

A different way to control the electrical conduction is to add small amounts of material, called dopant. In this process we want to add atoms with valence 3 or 5 into the lattice. If we choose a dopant with 5 valence electrons, they form a covalent bond with neighbouring atoms with covalent 4. The fifth electron moves easily through the lattice and form a set of discrete donor states just below the conduction band. Due to an excess of negative charge carriers (electrons) this material is called n-type semiconductor. Alternatively if we use a doping material with 3 valence electrons, it will produce a covalent bonds with four neighbouring atoms in the crystal which form an excess of holes. These form acceptor states just above the valence band, and its dominated p-type semiconductor as the primary charge carriers are the positively charged holes [21, 22].

It is important to have present that the n-type and p-type designation represents the sign of the charge of the primary carriers of the electric current. When n-type and p-type materials are brought into contact, the electrons from the n-type material can diffuse across the junction into the p-type material and combine with the holes. In the proximity of the junction the charge carriers are neutralized creating a region called the depletion region. The diffusion from electron and holes creates fixed donor or acceptor sites respectively, from the n-type region we have ionized particles and from p-type region it leaves behind negatively charged particles. The space charge from the fixed sites creates an electric field which eventually "halts further migration" [11].

When the radiation enters the depletion region it creates electron-hole pairs, and as a sequence the electrons flow in one direction, the holes in the other (as shown in fig. 3.1), and the total number of electrons collected can form an electronic pulse whose amplitude is proportional to the energy of the radiation. The detectors are operating with reverse bias voltage, which has two effects, increases the magnitude of the electric field in the depletion region and making charge collection more efficient, which increases

the dimension of the depletion region by forcing more carriers to drift across from one type of material to other [11, 21].

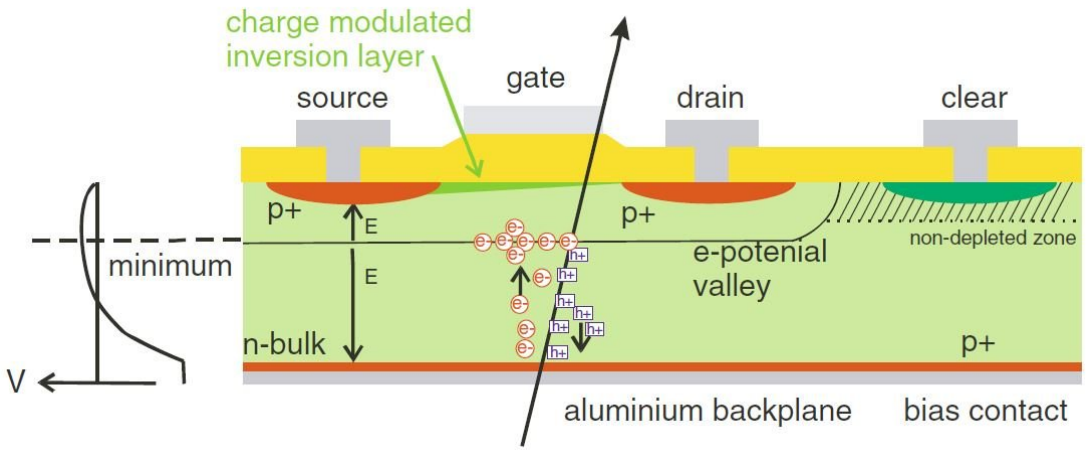

FIGURE 3.1: Schematic representation of a Silicon detector. The volume is depleted from the side n+ strips down to the back p+ implantation side [21].

3.3.2 Silicon detectors

Silicon detectors are widely used in experiments in particle and nuclear physics and for about half a century, the Silicon sensors and detectors have been used in high and low energy physics. They have been continuously improved to face new requirements and challenges. Based on a simple detection principle many different types of Silicon detectors have been developed. The detector technology is mostly based and applicable for tracking detectors, it means for detectors which measure the position of charged particles. From this information, track reconstruction software from the experiments deduces many parameters. These parameters include not only the flight path of particles, but also the kinetic energy, the momentum of the particle, the precisely measure of decay vertices, a fast response and a coverage of a full solid angle. In some experiments Silicon detectors are used as the active layers in sampling calorimeters. The first ever Silicon microstrip detector for particle physics, a surface barrier sensor, was tested in 1980 (Heijne, 1980) [21], and the first Silicon detectors using the planar technology and implanted strips were installed in the NA11 fixed target experiment at CERN in 1983 (Hyams, 1983) [23].

Silicon is the dominant semiconductor material used in the production of position sensitive detectors for particle physics. The moderate band gap between the conduction and the valence band is 1.12 eV. Therefore cooling is necessary only in ultra-low noise applications or when required to mitigate radiation damage. The detection of minimum

ionizing particles (MIP) is based on ionization or excitation of atoms in the medium caused by the passage of charged particles. The energy required to create an electron-hole pair is 3.6 eV yielding an ionization of about 80 eh/μm [21]. Thus Silicon detector can be quite thin compared with gaseous detectors.

3.3.3 Silicon interactions with heavy charged particles

This thesis retreats, as mentioned in abstract and along the text, a nuclear instrument equipped with Silicon detectors (see fig. 3.2), which aiming at detecting heavy charged particles. These particles, such as the alpha particle, interact with matter first through Coulomb forces between their positive charge and the negative charge of the orbital electrons within the atoms of the detector material. Despite of the fact that interactions between particles and nucleus are possible, its contribution is normally not significant. After the incident particle enters the detector, it immediately interacts simultaneously with many electrons. The attractive Coulomb force for the passing particle through the detector material is sense by an impulse on constitutive electrons. Depending on the collisions distance, this impulse may be sufficient to promote the electron to higher shell within the absorber atom (excitation) or to remove completely the electron from the atom (ionization). The transferred energy that is transmitted to the electron must come at the expense of the charged particle, and it's velocity is therefore decreased as a result of the reaction. The energy loss of a charged particle in a material is described by the BetheBloch formula (eq. (3.1)).

$$-\frac{dE}{dx} = 4\Pi N_A r_e^2 m_e z^2 \frac{Z}{A}\frac{1}{\beta^2}\left[\frac{1}{2}\ln\frac{2m_e c^2\beta^2\gamma^2 T_{max}}{I^2} - \beta^2 - \frac{\delta}{2}\right] \tag{3.1}$$

In this formula N_A is the Avogadros number, r_e classical electron radius, m_e the electron mass, z is the charge of the incident particle, Z the atomic number, A the mass number, T_{max} the maximum kinetic energy which can be transmitted to a free electron in a single collision, I the mean excitation energy, c speed of light, $\beta = \frac{v}{c}$, $\gamma = \frac{1}{\sqrt{1-\beta^2}}$ and δ the density effect correction. Every detector must be able to keep its noise well below a certain energy to be able to detect an minimum ionizing particles.

The maximum energy loss is about 1/500 of the particle energy per nucleon. Because this is a small fraction of the total energy, the primary particle must lose its energy in many such interactions during its passage through the detector. Furthermore, the number of interactions with electrons increases, so the net effect is to decrease its velocity continuously until the particle is stopped.

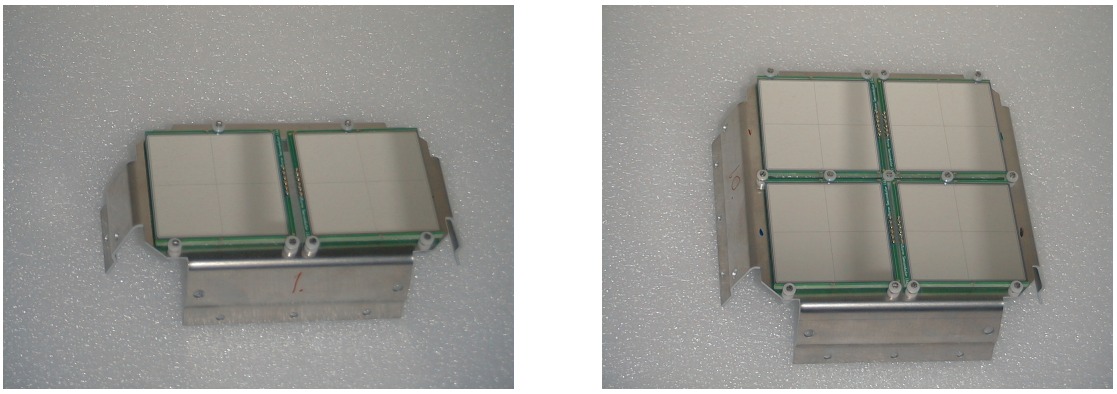

(a) (b)

FIGURE 3.2: Photos of Si-ball detectors with boards with 2 detectors (a) and boards with 4 detectors (b).

Once the basic properties of radiation detectors and the specific working principles of Silicon detectors have been presented, we move on to the description of the experimental apparatus around the detector system (Si-ball) on which the thesis is focused.

3.4 Scattering chamber, circuitry, electronics and cooling

Any detector system needs special conditions that are essential for its normal operation. Such conditions provided by the electronics, the circuitry, the chamber and associated tools.

The Si-ball chamber (see fig. 3.3) was specially designed and structured to perform nuclear experiments, paying special attention to the fact the Si-ball should be easy to manage and mount. The dimensions of the chamber are specifically suitable for the size of the Si-ball structure itself as well as any handling constituent tools from Si-ball when a experiment is performed. This chamber has several inputs completely sealed, preserving the desired vacuum conditions. Two inputs are reserved for the beam and for the vacuum system. In addition a movable side inlet where the structure of Si-ball is mounted and coupled in order to facilitate the access into the chamber and the Si-ball detectors.

The flange that closes this movable side contains also the connectors that allow the transmission of the electric signals from the detectors placed in vacuum to outside the chamber. These 18 pin-connector (a representative view is shown in fig. 3.4, are specially designed for signal transmission and low pressures conditions. The 18 pins allow for the simultaneous transmission of the signal from each quadrant for four detectors. The

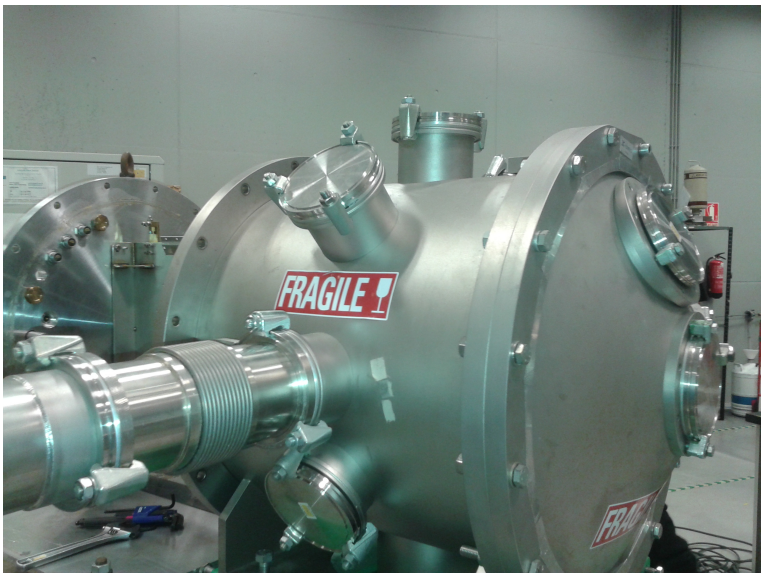

FIGURE 3.3: Si-ball reaction chamber at the end of the nuclear physics line at CMAM, with multiple entries and designed for different purposes [13].

cables that goes directly to detectors should be soldered on the connector side. As there are only 18 pins the 4 ground cables (black color) have to be soldered together 2 by 2.

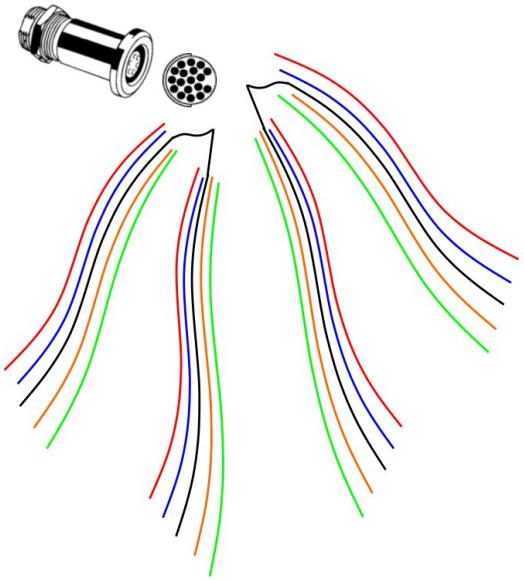

FIGURE 3.4: Schematic drawing of the cabling from Si-ball detectors connected to a feed through connector located in one of the flanges of Si-ball.

The electronic chain is the main signal modulation system needed for proper analysis. The electronic chain of Si-ball comprises the following modules: A MHV-4 voltage source, a pre-amplifier MPR-16 and STM-16 amplifier (or an MPR-64 module, which merges the the pre-amplifier and amplifier) of Mesytec company [25], an ADC (Analogic to Digital

Converter) V785, a TDC (Time to Digital Converter) V1190A, a scaler N1145, one NIM-ECL N638 conversion module, a dual timer N93B, a logic module N405, a fan-in fan-out (FIFO) N454 and gate and delay generator V830 all from CAEN company [26], and finally a MVME [27].

In the following we present some of the elements part of the electronic chain of a system of Silicon detectors, with a specific mention to the elements present in Si-ball electronic chain.

- **Pre-amplifier**

  The function of the pre-amplifier is to generate a pulse from the electrical current created by the detectors, introducing as little noise as possible, with suitable impedance so that it is not distorted later. Therefore, pre-amplifiers are generally physically placed close to the detectors to avoid any distortion of the signal before being processed. The MPR-16 [28] series provides a switch to amplify the output signal by a factor of 5. This helps to provide large output signals even at low charge depositions and thus provides good noise rejection.

- **Amplifier**

  Once the signal has gone through the pre-amplifier, it is brought to the amplifier to increase the signal significantly and process its shape. This process is needed as usually the signal coming from the pre-amplifier has a long tail of μs of duration that can produce several overlapping signals (pile-up). Processing also eliminates signal tails and improves the ratio between the signal and the noise. The mesytec STM-16 [29] is a shaping timing filter amplifier with discriminator and multiplicity trigger specially designed for single or double sided multistrip Silicon detectors. It can best be used in conjunction with the preamps of the mesytec MPR-Series.

- **Fan-in Fan-Out (Fi/Fo)**

  Fan-in Fan-out, or FIFO module is a module that allows adding signals in the input channel (fan-in) or dividing an input signal into multiple outputs (Fan-out) of the same shape and amplitude. This is necessary when you want to make several processes with the same signal. The module N454 [30] is a single width NIM unit housing 4 independent Fan In-Fan Out sections. Each section accepts 4 input NIM signals and performs on these the logic OR function. The result of the function is available as 4 normal and 2 complementary NIM signals on 6 front panel connectors. The unit can be programmed, via a front panel switch, to work as 4 OR sections (4 inputs/4 outputs) or 2 OR sections (8 inputs/8 outputs).

- **Logic module/logic pulses**

  The logic modules allow processing various signals and impose a function logic based on the value of these signals. These logical functions are AND and OR. An AND operation is one that gives a signal positive long as all the input signals are positive and gives a null signal when any of the input signals is zero. A OR operation is one that gives a signal if any of the input signals is positive and gives no signal if all the input signals corresponds to a a logic zero. The module N405 [31] is a one unit wide NIM module housing three independent sections that can be used either as logic unit or majority. The two modes are selectable via internal DIP switches. Each section accepts 4 input signals, a VETO input and provides 4 outputs (2 normal and 1 complementary, shaped, plus 1 linear). The linear output provides a signal whose width is equal to the time during which the input signals satisfy the conditions programmed via the front panel lever switches. The shaped output widths can be set via front panel trimmers in the range 6 ns to 800 ns.

- **NIM-ECL/ECL-NIM Translator and Fan Out**

  The NIM-ECL Converter is a module in which the signal are converted either from NIM standard to ECL and vice-versa. The NIM-ECL Converter is a cost-effective solution where only a small number of signals require level translation. The module N638 [32] is a standard NIM module housing 16 independent logic level translators. Each of the 16 channels accepts a NIM or an ECL signal and provides two NIM and one ECL outputs. The NIM and ECL inputs of each channel are OR prior to fan-out. The maximum operating frequency is 300 MHz.

- **Gate and Delay Generator**

  A Gate Generator is a module that produces a logic signal with a certain width given the arrival of a start signal. Normally, this signal open a time window (gate) which is used by the acquisition to accept other signals. The produced gate signal may be delayed by the Delay Generator. In addition to this direct application, these modules can be conveniently used for other purposes such as generating a trigger. The model V830 [33] is a 1-unit wide VME 6U Multievent Latching Scaler, housing 32 independent counting channels. The maximum input frequency is 250 Mhz. The counters values can be read on the fly from the VME without interfering with the data acquisition process. The Trigger signal can be provided by an external NIM/ECL signal or by a VME request. It is also possible to generate a periodical Trigger signal by means of an internal programmable timer. The board has a special circuitry that allows it to be removed from or inserted in a powered crate without switching the crate off.

- **Scaler**

  A Scaler is a module that counts the number of input signals it receives. Thus, information can be obtained about the number of events registered. The module N1145 [34] is a double unit NIM module that includes four independent 8-digit counters each with their own display and can accept up to 250-MHz input rates. These counters can be cascaded to increase the word length to 16-digits for two counters, and 24-digits for three counters. Counters 2 and 4 have a "Carry" or overflow output to allow the cascading of the counters. Counters 1 and 3 have a set of bridged gate connectors to allow a single gate to be used on multiple counters.

- **Analog to Digital Converter (ADC)**

  Once each signal has been amplified and processed, it reaches the ADC in which the amplitude of the pulse (which is the parameter that carries the information on the energy left by the particle in detector) is converted into a number (digital signal). The model V785 [35] is a 1-unit wide VME 6U module housing 32 Peak Sensing Analog-to-Digital Conversion channels. Each channel is able to detect and convert the peak value of the positive analog signals (with <50 ns rise-time) fed to the relevant connectors. Input voltage range is 0 to 4 V. The outputs of the PEAK sections are multiplexed and subsequently converted by two fast 12-bit ADCs (5.7 s for all channels). Programmable zero suppression, multievent buffer memory, trigger counter and test features complete the flexibility of the unit. The board supports the live insertion that allows inserting or removing them into the crate without switching it off.

- **Time to Digital Converter (TDC)**

  As in the case of the ADC, where the pulse amplitude is recorded, TDC records the timing of the arrival of the pulses along the data acquisition window. This way you can obtain the temporal position of each event (taking into account delays suffered signals along electronics chain and the Gate and Delay Generator Generator if present). The V1190A [36] is a 128 channel Multihit TDC, housed in a 1-unit wide VME 6U module. The unit features High Performance Time to Digital Converter chips developed by CERN.

- **Trigger Pulse Generator (dual timer**

  Trigger pulse generators usually allow the control of the pulse repetition rate (frequency), pulse width, delay with respect to an internal or external trigger and the high- and low-voltage levels of the pulses. More-sophisticated pulse generators may allow control over the rise time and fall time of the pulses. Pulse generators are available for generating output pulses having widths (duration) ranging from

minutes down to below 1 picosecond. The module N93B [37] is a one unit NIM module housing two identical triggered pulse generators. The module produces NIM and ECL pulses whose width ranges from 50 ns to 10 s when triggered. Output pulses are provided normal and complementary. Timers can be re-triggered with the pulse end marker signal. The coarse adjustment of the output width is provided via a 10-position rotary switch, the fine adjustment can be performed via a rotary handle. The trigger START can be provided either via an external signal or manually via a front panel switch.

One of the tools which could be used to improve the signal from the detected particles is a cooling system. Silicon detectors like the ones which are part of Si-ball need adequate cooling. The cooling system has fundamental properties that are helpful on the consisting experiment. The Silicon detectors are highly heated due the exposition of high radiation doses which can damage the Silicon crystal lattice. To relieve from this conditions of this radiation damage, the Silicon detectors much be kept to sub-zero (°C) temperatures at all time. One of the primary consequences of radiation damage of Silicon detectors is the increasing of leakage currents inside the Silicon, which cause additional heating, resulting in a thermal runaway of the sensor when not adequately cooled. Cooling fluids in detectors are also subject to radiation doses and need thus to be resistant as well. Up to now fluorocarbons are used frequently both in single and 2-phase. Normal HFC refrigerants are not radiation resistant and therefore cannot be used as such [38].

As mentioned above Silicon detectors are required to be as light-weight as possible, to avoid deflection of particle tracks. However the mass of cooling hardware (tubes and fluid) tend to make a significant contribution to the overall material budget. The figure below (fig. 3.5) show the cooling machine used for Si-ball. At the moment it is not operating.

FIGURE 3.5: Cooling system of Si-ball, which could provide a low temperature directly to detectors.

The next section will show and present the performances and characteristics of Si-ball detectors.

3.5 Performances and characteristics of detectors according to manufacturer

The detectors constituting the Si-ball are provided by Micron Semiconductor Ltd. [24], and manufactured on n-type Silicon with $< 100 >$-crystal orientation and resistivity above 15 kΩcm. The average active thickness is 988±6 μm, fully depleted at around 200 V. In this way the energy of fully stopped protons ranges from below 100 keV to 12 MeV. These MSQ25-1000 type detectors are mounted in a PCB (see fig. 3.6) transmission package specially designed to minimize dead areas. The dead-layer and entrance window thickness have been reduced to allow for the reduction of the detection thresholds.

These are the general characteristics of Si-ball MSQ25-1000 type detectors:

Table 3.1: General characteristics of Silicon detector performing in Si-ball

SILICON DETECTOR TYPE	QUADRANT DETECTOR
DESIGN	Totally depleted ion implanted structures with multi-guard rings for over voltage operation.
PART DESIGNATION:	MSQ25-65, MSQ25-140, MSQ25-300, MSQ25-500, AND MSQ25-1000
TECHNOLOGY:	4 INCH SILICON
N° of ELEMENTS:	4
N° of OUTPUTS:	5
ELEMENT ACTIVE AREA:	2500 mm^2
TOTAL QUADRANT SECTOR AREA:	24.975 x 24.975 mm^2
QUADRANT SECTOR,SEPARATION:	50 μm
CHIP DIMENSIONS:	52.02 x 52.02 mm^2 53.02 x 53.02 mm^2 57.02 x 57.02 mm^2
THICKNESS:	65 μm, 140 μm, 300 μm, 500 μm and 1000 μm
FULL DEPLETION,OPERATION VOLTAGE:	10-250 V Subject to thickness
RISE TIME:	50 ns maximum
RESISTANCE:	1 MΩ
RESOLUTION (Am 241):	Junction 55 keV typical, 75 keV maximum FWHM Ohmic 75 keV typical, 100 keV maximum FWHM
QUADRANT SECTOR NOISE:	15 keV FWHM (1 μs TC)
ELEMENT (μs T.C):	20 keV
METALLISATION:	Aluminum 3000 $\AA$
CONTACTS:	Metallisation on the active area element 100% metallisation on back
MINIMUM ACCEPTANCE	100% elements operational

These are the general characteristics of detector's PCB.

TABLE 3.2: PCB STANDARD

Material	FR4
Thickness	1.6, 2.4 or 3.2 mm
Dimensions	70 x 70∼mm^2
Mountings	4 holes 25 mm at corners
Aperture	50 x 50∼mm^2
Connectors	Cambion 460-1521-02-03-00
Connections	4 to active area, 2 to ground

TABLE 3.3: PCB CUSTOM

1.	Material	FR4
	Thickness	2.4
	Dimensions	59 x 59 mm^2
	Aperture	50 x 50 mm^2
	Connectors	Cambion 460-2599-04-03-00
2.	Material	FR4
	Thickness	1.6, 2.4 or 3.2 mm
	Dimensions	5.4 x 55.4 mm^2
	Aperture	50 x 50 mm^2
	Connectors	Cambion 450-3703-01-03-00

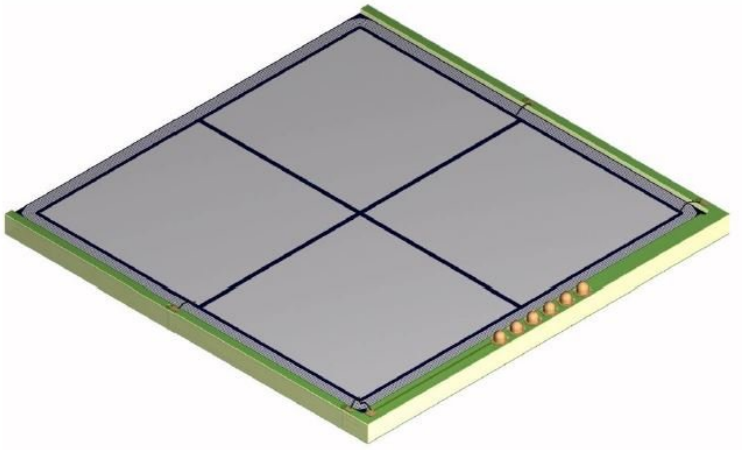

FIGURE 3.6: Silicon Detector type MSQ25-1000 with PCB custom package 2.

After the specifications of the detectors which are part of Si-ball have been presented, we show and explained the geometry of Si-ball detector.

3.6 Geometry of Si-ball

The Si-ball geometry is based on a structure with an apothem of 16 cm, 4 square plates (119x119 mm^2) containing 4 detectors and 8 rectangular plates (119x59.5 mm^2) with

two detectors. The basic geometry concept and structure are shown in fig. 3.7. Each square plate is covered with four Silicon detectors 51x51 mm^2 and each segmented into quadrants of 22.5x22.5 mm^2, as we could see in fig. 3.8. The solid angle subtended by each quadrant is about 0.21% of 4π. The assembly makes a total of 36 detectors (4x5 + 8x2), and 144 channels (36x4), or energy signals.

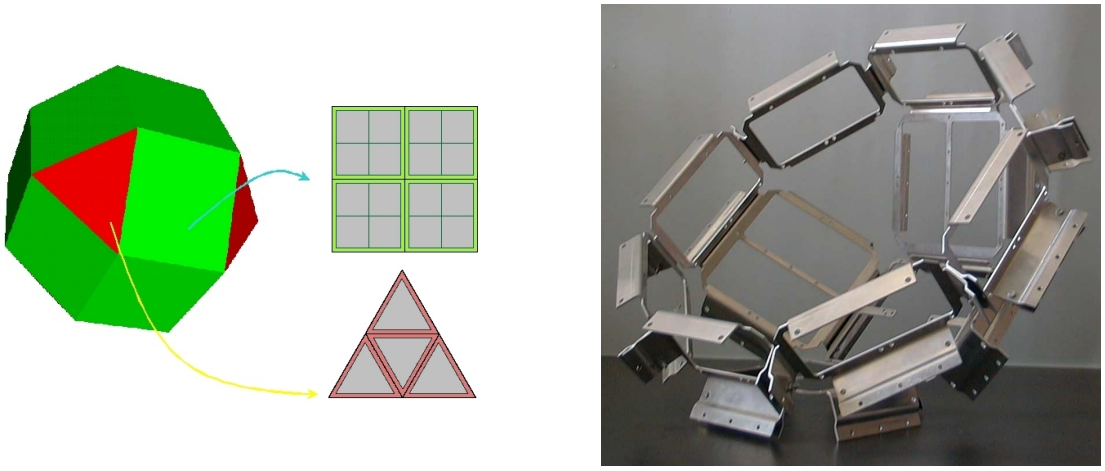

(a) (b)

FIGURE 3.7: (a) Si-ball design for quadratic detectors and triangule detectors with a rombicuboctaedric shape. (b) Real Si-ball strucuture in a semi-rombicuboctaedric shape with some of detectors now grouped in pairs [1].

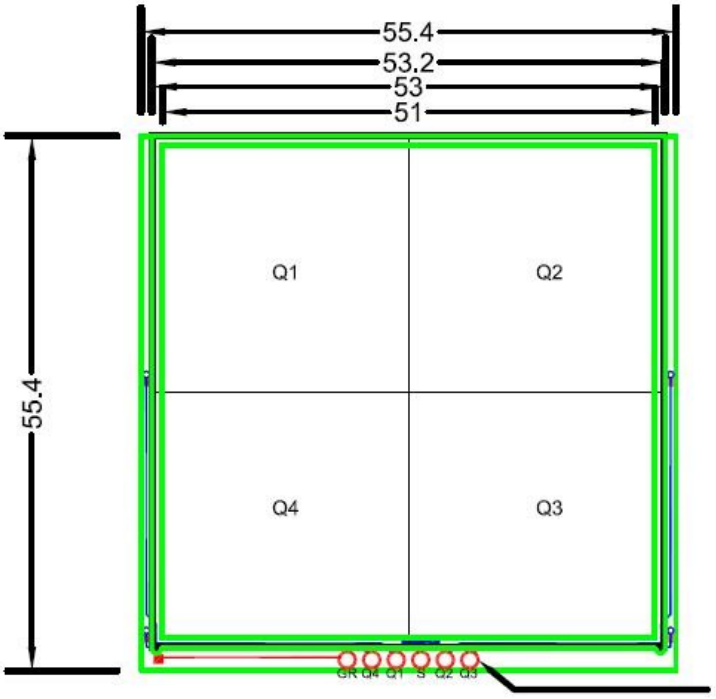

FIGURE 3.8: Scheme of one detector from Si-ball with the designated quadrants and based on a PCB.

The active thickness of the Si-ball detectors is 988 μm (with a Silicon dead-layer of 0.8 μm, according with the manufacturer) and operates with a voltage of -250 V, to get a full depleted active region, improve signal-to-noise response, increase detection efficiency, improve energy detection resolution, etc. The time of flight of 2 MeV α particles along the Si-ball radius is 16 ns, for 8 MeV α particles it is 2.3 ns. These values are significantly different from those characteristic of a proton at the same energy, 8 and 1,15 ns for 2 and 8 MeV respectively. The Si-ball was projected to achieve the following goals:

- By combining multiple Silicon detectors get a wide-angle coverage.
- Considering the thickness of the detector it is possible to detect charged particles in a wide range of energies (protons can be detected from 100 keV up to 12 MeV).
- Due to the large number of detectors, the system has a large granularity allowing for a precise reconstruction of the trajectories of the detected particles.
- The high granularity allows the study of various particle emission channels.
- The design is light, due to the aluminum mounting frame.
- The radius of the structure (16 cm) allows time of flight studies.
- The detectors can be cooled to reduce noise and improve its energy resolution.
- The design allows the use of the device both in decay experiments β as in nuclear reactions.

For calibration calculus we must take into account the energy loss of the inert particles in the dead-layer of detectors (0.8 μm for Silicon Ball detectors) which depends on the effective thickness traversed by the particle which in turn depends on the angle of incidence of the particle with respect to the normal detector. To calculate the angle is not necessary to know only the position of the detection point, but also the normal to the detector. Due to detector placement and choice of the coordinate axes, all are 45 degrees or normal to any axis, which makes simple the calculation of these normal vectors to surfaces.

We shall now describe in the next section a brief description of detectors dead layer.

3.7 Detector's Dead Layer

Semiconductor detectors in general have a dead-layer at their surfaces that is either a result of natural or induced passivation or is formed during the process of making

the metallic contact. Charged particles passing through this region produce ionization that is incompletely collected and recorded,resulting in worst energy deposition and resolution.

Semiconductor detectors have in their surface dead-layers in which ionizing particles can deposit energy, creating charge which is incompletely collected by the readout electronics. These layers correspond to the doped regions defining the semiconductor properties of the device, ohmic contacts to bias voltage and readout electronics and/or undepleted volumes of under-biased detectors. Dead-layer effects have received detailed attention in the spectroscopy of low-energy gamma and X-rays, which deposit energy in or near the dead-layer. Similarly, for charged particles, energy loss in even the thinnest of dead-layers can amount to a significant fraction of the total energy deposition for radiations of interest in nuclear and particle physics experiments. For example a 20 keV electron can deposit approximately 1% of its total energy in a 100 nm Silicon dead-layer [39].

The procedure is well explained by the time when a charged particle enters, the diode surface interacts with the diode medium. The particle will continuously loose energy and generate electron-hole pairs along its track. The electrons generated in the neutral p region must diffuse to the depletion region before being collected. The time for this diffusing process can be significant with respect to electron lifetime, and recombination may occur.

Overall the insulation film, aluminum electrodes, and P-layer of the Silicon detector surface serve as dead-layers causing an energy loss to the incident particles, but the energy loss that does not result in signal generation.

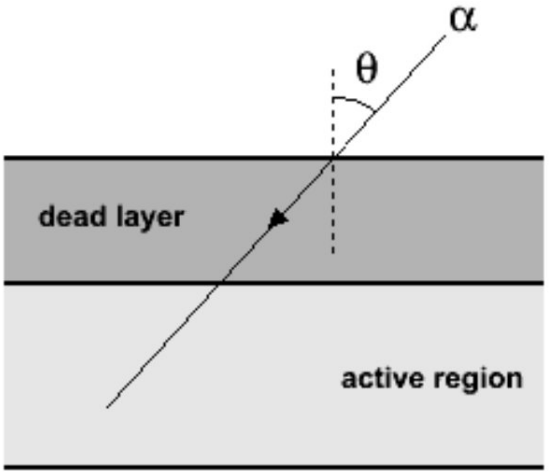

FIGURE 3.9: Scheme of a detector with dead-layer and the active region.

This fact influences not only the final energy resolution of the detector, but implies some issues in the correct energy calibration of the detector which needs to be taken into consideration. As we can observe on fig. 3.9, the amount of energy lost by the particle in dead layer directly depends on its entrance angle (with respect to the perpendicular plane of the layer), resulting in non-negligible differences in the final deposited energy affecting the energy resolution and calibration.

Considering all the information presented in the previous chapters, the following chapter will present the goal of the present thesis, the characterization of the thickness of the dead layer of the individual Si-ball units.

Chapter 4

Experimental setup and data analysis for estimating dead-layer and thickness

This chapter presents the core of the experimental work performed within this Master Thesis at CMAM and CSIC laboratories. After all information collected and described in the previous chapters, we move on to the characterization of the individual Silicon detectors units of Si-ball and their calibration for future experiments. The progression of the work is provided in sequential sub-chapters. All the steps and tools used for dead-layer estimation are particularly described. Section 4.1 provides an overview of the different components of the test bench used in this work. Details on the vacuum chamber and associated cabling (4.1.1), the electronic chain (4.1.3), radioactive sources and collimating systems (4.2.2) are given along the first section. The utilized data acquisition and analysis system, as the methodology and various considerations adopted to perform the measurements are shown on section 4.2, followed by the analysis and interpretation of the obtained data that allowed the estimation of the dead-layer thickness in the Si-ball detectors.

4.1 Experimental setup

This section presents the various hardware and software components that form the test bench implemented in order to characterize the detectors of Si-ball. A scheme of the experimental setup is shown in fig. 4.1. Each of its modules will be introduced in the following subsections, together with the components to detect the alpha particles from α sources (referenced on subsection 4.1.2). All parts are essential elements needed to

obtain the correct calibration parameters that permit the estimation of the dead-layer of the detectors and its consideration in future experimental campaigns.

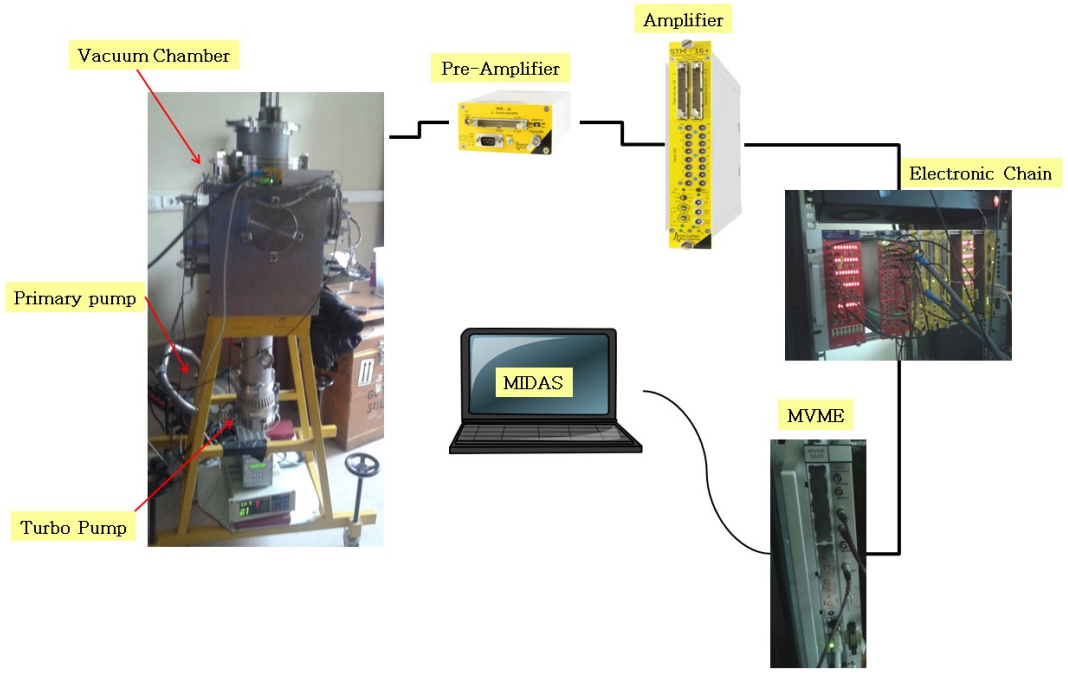

FIGURE 4.1: Schematic drawing of the experimental setup used in the characterization of the dead-layer thickness of the Si-ball detectors.

The main work presented, which consisted on mounting the test bench and perform measurements to estimate the dead layer thickness of detectors, was carried out at CSIC, where the Si-ball detectors were calibrated and characterized in detail. The detector system was then moved to CMAM where it was mounted and prepared to be operational.

4.1.1 Vacuum chamber and connections

The vacuum chamber of the test bench (a photograph is shown in fig. 4.2) is a mechanical element where detectors and part of the electronics are placed. Because of the working conditions of the Silicon detectors and the nature of the measurements itself, the chamber must be sealed from the surrounding atmosphere, at typical pressures $\sim 10^{-7}$mbar. As shown in the figure, some ports are enabled in order to access to the interior of the chamber. Removable flanges in the ports permit to open and close them. A very advanced vacuum technology is needed for coping with this situation where the gradient of pressure from the inside to the outside of chamber is typically of 9 order of magnitude while electrical signal as weak as ten milivolts must driven from the detectors (inside the chamber) to the electronic modules (outside the chamber).

In case of CSIC the chamber are not connected to an acceleration line since we are using radioactive α sources instead of an ion beam for the detectors characterization. So the chamber has an air channel to vacuum system, and 3 other flanges that are closed. One of them has the cable connections to let the signal get through and be processed by electronic chain and finally analysed at the acquisition system. This particularly stamp has one cable that are highly developed for lower pressures, this is, pass the detector signal from low pressures to atmospheric pressure, and is dominated feethrough. One other serves to help when its needed to get in or out the detectors, and the upper stamp, that is directly attached with the detector, make possible the positioning of them.

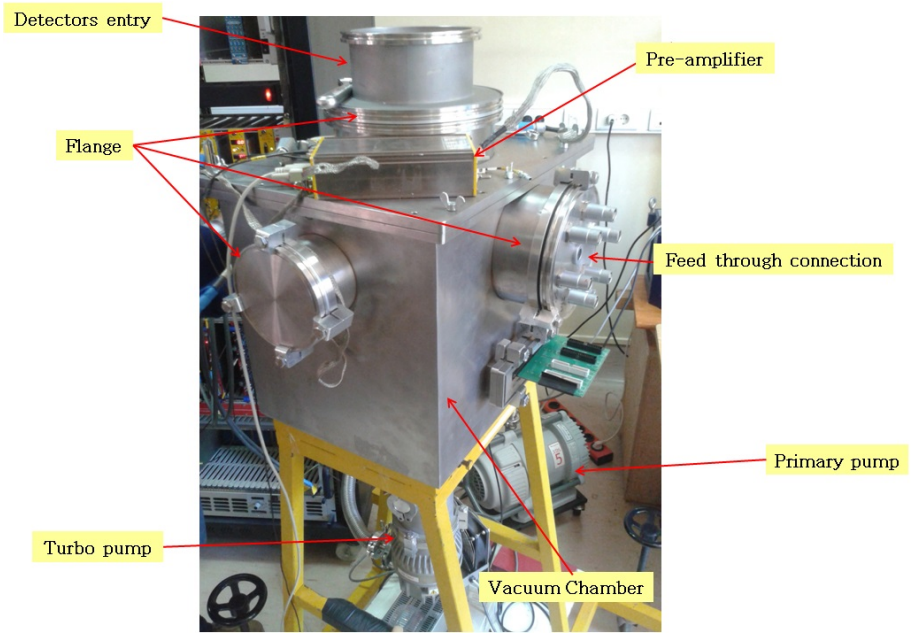

FIGURE 4.2: External view of the scattering chamber used during the characterization of the dead-layer of the Si-ball units. In the lower part of the picture the associated vacuum units can also be seen.

So the primary pump (picture (a) of fig. 4.3) lows the pressure around 10^{-1} mbar (knowing the atmospheric pressure is $\sim 10^{3}$ mbar) and the second pump, turbo pump (picture (b) of fig. 4.3), reduce it significantly in the order mentioned before, $\sim 10^{-7}$ mbar.

The pressure Gauges allows for measuring the pressure inside the chamber. Varians senTorr Gauge Controller (a photograph is shown in fig. 4.4) is a complete, half-rack vacuum gauge controller that offers continuous, reliable pressure measurement from rough to high vacuum. The controller comes completely configured from the factory to operate one of six independent gauges. The upper instrument (we can see in fig. 4.4) is the controller of the turbo pump, that turns on/off and select the configurations.

(a) (b)

FIGURE 4.3: Primary Pump (a) and turbo Pump (b) used for reach the pressure pretended to the characterization of Silicon detectors from Si-ball. At the left picture is also seen the Gauge controller.

The senTorr Gauge Controller features one digital display per gauge tube, that is directly connected to the tube that came out directly from the chamber to turbo pump. The front panel keypad are equipped with lockout features that prevents against unauthorized parameter inputs. The analog outputs and remote capabilities are located on the back panel. The high-vacuum gauge emission can be controlled with external input controls that turn on when we want to reach at low pressure levels or turn off when we want to stop the vacuum and open the chamber. The senTorr offers an extraordinary amount of gauging and programming capability which are easy to use. It is easily accessible to all of the instrument's functions and parameters through the front panel keypad or the optional serial link.

4.1.2 Radioactive sources and collimator

Many heavy nuclei are energetically unstable against the spontaneous emission of an α particle. The probability of decay is governed by the penetration barrier mechanism described in most nuclear physics texts [11]. The spontaneous emission of an α particle can be represented by the following process:

$$ {}^{A}_{Z}\mathrm{X}_{N} \rightarrow {}^{A-4}_{Z+2}\mathrm{X}'_{N-2} + \alpha \tag{4.1} $$

FIGURE 4.4: Vacuum controller (senTorr Gauge Controller). This device allow to control the pressure inside the chamber in order to reach the specific conditions of the experiment.

The particles are emitted individually or in groups with well defined energies. These are the general cases where occurs a transition, in which the α particles are emitted to a particular energy. Most α radioactive sources emit particles with energies limited between 4 and 6 MeV, with typical half-lives in the order of several days to thousand years. Because of its double charge, $+2e$, α particles have a very high rate of energy loss in matter, and that is why α sources must be deposited on a substrate as thin as possible in order to minimize energy loss and auto absorption in the source. A thin layer of metal prevents encapsulated alpha sources for the contamination of the surrounding of the alpha emitter.

An important aspect in choosing a source for calibration is the number of particles used for calibrating that are emitted within a reasonable time interval for the particle detection not to be longer than desirable. This is determined by the activity of the source. The fact of having a good statistic associated with the number of counts, improves the quality of the spectrum as the reference for marking the calibration.

The radioactive alpha sources used in this work are: ^{148}Gd with energy of the emitted α particle 3182 keV, a triple-α source composed of ^{239}Pu, ^{241}Am and ^{244}Cm with energies of α particles 5156.59, 5485.59 and 5804.82 keV respectively, and a source of ^{210}Po which emits α particles with energy of 5304 keV. For the triple-α source it was only considered the ^{239}Pu peak because it presented more statistic and a well defined peak. The information relative to radioactive alpha sources is shown on the table 4.1.

The first step in system calibration is to characterize the effective thickness of the dead-layer. Were made individual measurements for each board, where were chosen 4

TABLE 4.1: Information of α sources isotopes

Isotopes	**Energy (keV)**	**Half-life**	**I (%)**
^{148}Gd	3182	74.6(30) y	-
^{210}Po	5304	138.376 d	-
^{239}Pu	5156	24.110 y	73.3
^{241}Am	5485	432.2 y	85.2
^{244}Cm	5804	18.1 y	76.4

different angles for each quadrant, in order to have various angles of incident α particles and thus have a wider sampling.

For precise detection of the particles, which are being emitted in 2 π, it was necessary to build a mask (see fig. 4.5) allowing us to accurate a determined incident angle. The mask has small holes (3 mm diameter) acting as collimators, each hole is in front of the middle of a quadrant. It shows the two types of mask used, either for 2 detectors or 4. With this last characteristic it is possible to get various angles measured at same time. The mask was placed at 0.5 cm of the detector and 8.25 cm of the sources, which make the distance between source and detectors be 8.75 cm. As the holes have 3 mm of diameter the angular resolution is $\pm 1°$.

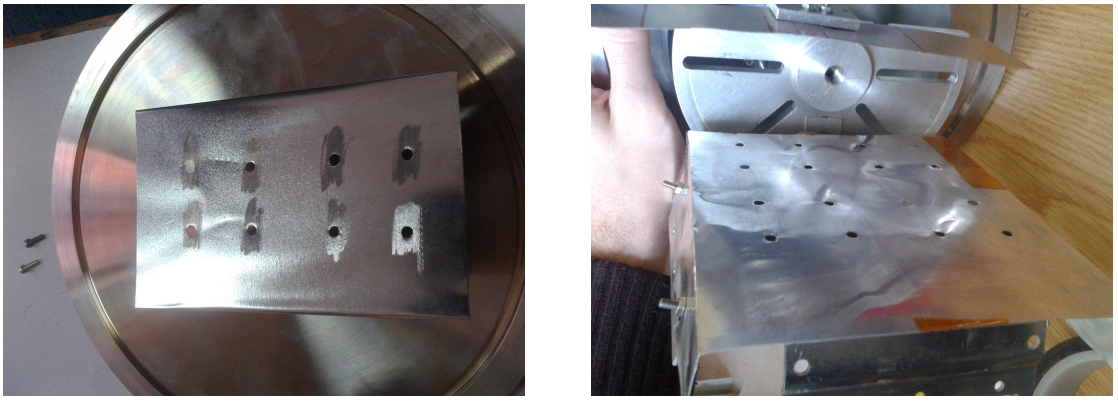

(a) (b)

FIGURE 4.5: Mask for board with 2 detectors (a) and four detectors (b) to collimate the incident particles.

We can see on fig. 4.6 the flange that attached the detector with the mask placed at front of it and the alpha sources. Its described the all objects which are part of the removable flange that facilitates the detectors and alpha sources access and positioning. In other hand is present other components that facilitate the control of the system, as the manipulator tube which can position the sources in upper and down direction, or the ring made with special material for high vacuum requirements.

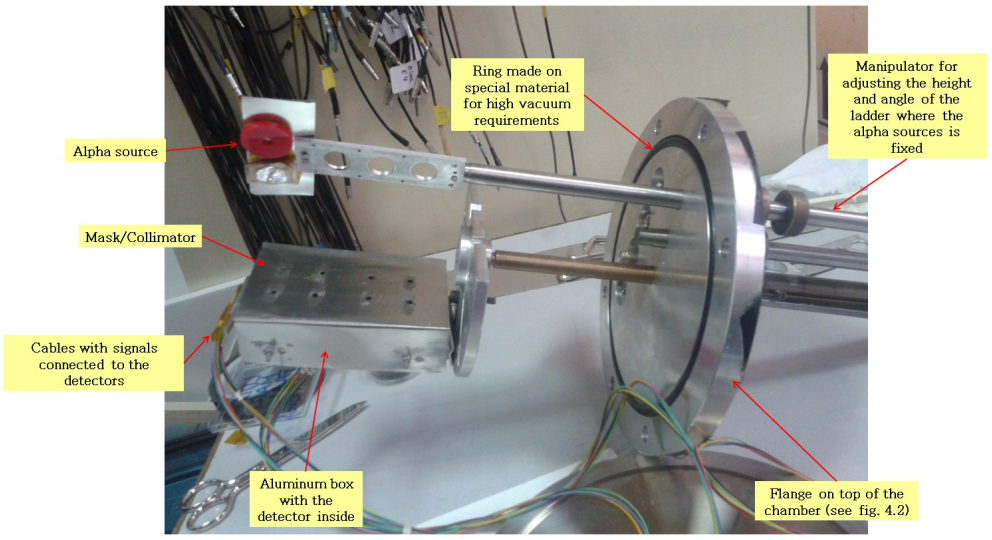

FIGURE 4.6: Alpha sources mounted in front of detector and the collimator mask attached to the removable flange.

4.1.3 Electronic chain

The fig. 4.7 illustrates the different electronics modules used in the test bench that treat the signal originated in the detector by a charged particle. Description of the modules can be found on section 3.4 of the chapter dedicated to Si-ball detector. The detectors are powered via coaxial LEMO cable, and in this particular experiment it was used a MHV-4 module power supply [40]. In our test bench, the modules where it is performed the shaping of the signal coming from the detector are a MPR-16 [28] pre-amplifier and a STM-16 amplifier [29]. Considering the signal from the detectors, the pre-amplifier generates a voltage pulse using a high-pass filter that suppresses the low frequency noise in the signal. The pre-amplifiers are typically placed nearby the detectors to avoid any possible distortion of the signal before being processed. The output of the pre-amplifier is brought through a 17 twisted pair flat cable to the amplifier, which delivers a gaussian-shaped output signal (analog output) significantly increased. It is necessary to adapt the shape of the pulses, because normally the signal from the pre-amplifier has a long duration (time duration of its tail ∼milliseconds) that can produce several overlapping signals. The form processing, so called "shapping", eliminates these tails and improves the signal to noise ratio. The amplifier produces two types of signal: **i)** analog, which is sent to the analog-to-digital converter, ADC; **ii)** timing, of ECL type, used for measuring time intervals; **iii)** logic, of NIM type, used for implementing the logic for event validation, for implementing the "trigger".

The logic modules used for the trigger implementation and the hardware used for implementing the required logic functions was: CAEN N454 (FIFO), CAEN N638 (AND/OR Logic Unit), CAEN N93B (Dual Timer) [26]. As shown in fig. 4.8, the

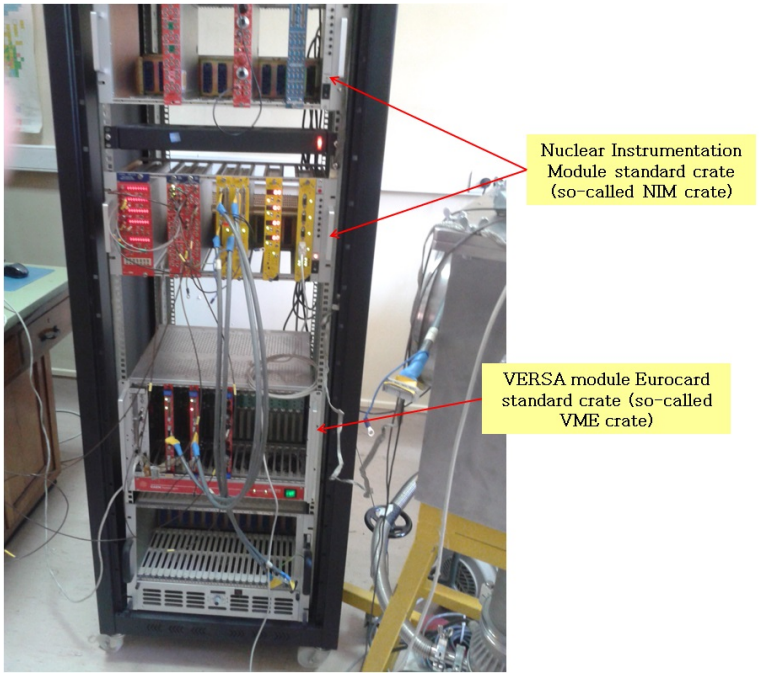

FIGURE 4.7: Electronic setup in operation at CSIC for alpha particles detection

logic signal produced by STM-16 is sent to a FIFO N454, Fan-in/Fan-out module. In practical terms, this modules delivers four copies of the input signal. The signal is then directed to logic modules N638. The logic modules allow the processing of various signs and impose a logic function based on the value of these signals. These logic functions are AND and OR. The signal is than lead to the Trigger pulse generator N93B (dual timer), as a trigger system that allows us to trigger when we are receiving signal and when it is a valid count.

To validate a count we made use of two electronic devices, the scaler N1145 and a gate/delay generator V830. The Scaler is a module that counts the number of input signals received from FIFO, i.e, provide the number of generated counts, and pass the information to trigger pulse generator which start the counting. The logic signal continues to Time to Digital Converter modules, essentially used for measure time intervals of the arrival of the pulses along the data acquisition window. The last logic module is the Gate Generator, which is a module that produces a signal duration given the arrival of an input signal. During the signal duration, the objective is to open a time window at which an event can be accepted by the data acquisition system. The signal may be delayed, by the Delay Generator, necessary to delay differences between signals. When the time interval ends it send back the information, to logic modules and the scaler, to accept another count.

Once the analog signal has been amplified and processed, it arrives at the ADC module V785 [26] where the amplitude of the pulse, which is the parameter and where

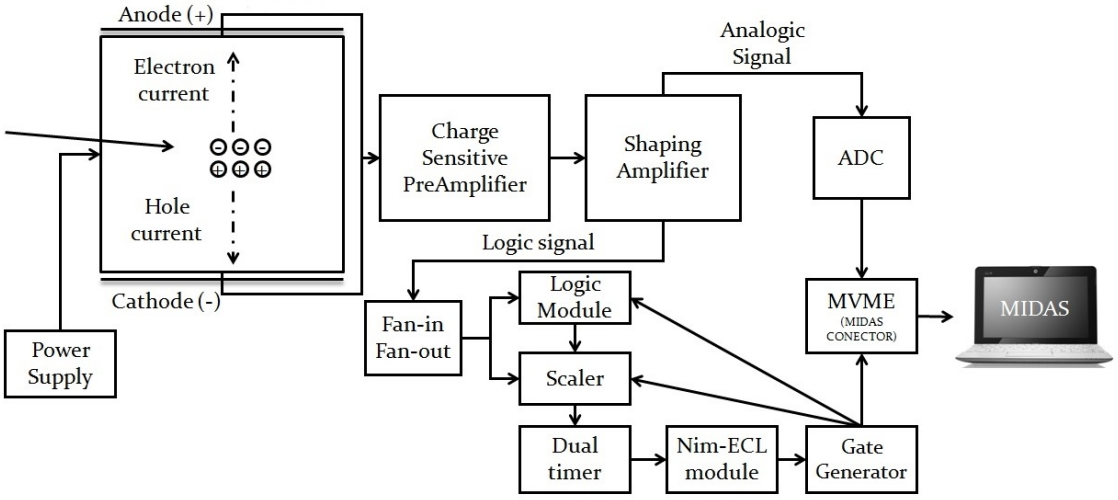

FIGURE 4.8: Electronic chain scheme with the designated electronic components right demonstrate since the *alpha* particle detection until the signal reach the MIDAS software.

contains information left by the particle is converted into a number (digital signal). Normally the maximum value of the input signal is taken as the amplitude, and therefore the value is interpreted as the particle energy. The last modules are connected to MVME, which transmits the data to the software of the acquisition system.

The electronics system operating in the test bench work with two types of non-analog signals: NIM (Nuclear Instrumentation Methods) and ECL (Emitter Coupled Logic).

The goal of NIM standard is to promote the interchangeability of instrumentation modules for easy mounting setup. It provides a common footprint for electronic modules (amplifiers, ADCs, DACs, discriminators, etc.), which plug into a larger chassis (NIM crate, or NIM bin). The crate must supply 12 and 24 volts DC power to the modules via a backplane. They can, however, also be built in multiples of this standard width, that is, double-width, triple-width etc. The NIM standard also specifies cabling, connectors, impedances and levels for logic signals. The fast logic standard NIM logic, is a current-based logic, with negative true (at 16 mA into 50 ohms = -0.8 volts).

Other signal present is ECL-based logic. ECL is a high-speed integrated circuit bipolar transistor logic family.

To communicate with the acquisition system software is necessary a VMEbus. VMEbus (Versa Module Europa bus [27]) is a computer bus standard, which is a communication system that transfers data between components inside a computer, or between computers. This expression covers all related hardware components (wire, optical fiber, etc.) and software, including communication protocols. In our setup we used an MVME

(Motorolla VME). As a consequence, NIM-based ADC modules are nowadays uncommon in nuclear and particle physics. NIM is still widely used for amplifiers, discriminators, nuclear pulse generators and other logic modules that do not require digital data communication but benefit from a backplane connector that is better suited for high power use. So to contact with the ADC are used a VME crate. The analogic signal is passed to ADC that communicates with VME.

Before proceeding with the acquisition of the produced signals, we will remind on the importance of the dead-layer in correctly calibrating of the considered Si-ball detectors.

4.2 Dead-layer thickness estimation

The previous chapter describes the experimental setup that was set for this experiment. The realization of the measures implemented in the same system are now described as the steps that have been taken.

The radiation detectors provide a current signal which is converted into a voltage signal. In general the response of the detector material is such that the current supplied preserves the characteristics of the incident radiation. In a semiconductor detector, the incident radiation interacts with the material of the detector (subsection 3.3.3), producing/creating electron-hole pairs (subsection 3.3.1). These pairs are collected by charged electrodes where the electrons move to the positive electrode and holes to the negative electrode, and thus create a current pulse. Upon arriving pulses provide information about the type of particle energy, arrival time or rate. Considering the case of Si-ball detection system, and because the wide angular coverage of the experimental system there is a strong angular dependence on the energy deposited by the heavy particles. This is because the thickness of the dead-layers of Silicon detectors used do cause a considerable loss of energy that depends on type of particle and its incident energy. Because of this, it is necessary to take into account the energy difference for different angles and different energies of the α particles, e.g. depending on the incident angle and the type of particles, discussed previously. At this stage of the work, we will introduce the calibration measurements performed with α particles of well known energies to correctly estimate their loss of energy before reaching the active volume of the detector where charge produce by ionization is collected.

4.2.1 Experimental method

In order to calculate the dead-layer thickness the experimental method take several steps to initiate the measurement. With only available space and connectors sufficient to one

board at a time, it was measured each board individually and each measurement took one hour difference from one to other, just to have enough statistic. Each hour/measurement represents one position measured, with the alpha sources displaced at front of the detector's quadrants. This positions are represented schematically above (see fig 4.9) with indication of the methods used to calculate the dead-layer thickness. Its is important to reference again that each position means a source placement at front of some quadrant individually and at specific angles from the others. The transference for the same method but different steps required the remove of the flange where the detectors and the sources outside, and change the position of sources. In total we have 12 boards, enumerated from 1 to 12, plus the board E, the boards are divided in 2 detectors in and 4 detectors in, so we have 8 boards with 2 detectors and 5 boards with 4. Each detector has 4 quadrants, which in total for all boards we have 144 quadrants, and for each quadrant we need 3 measured angles.

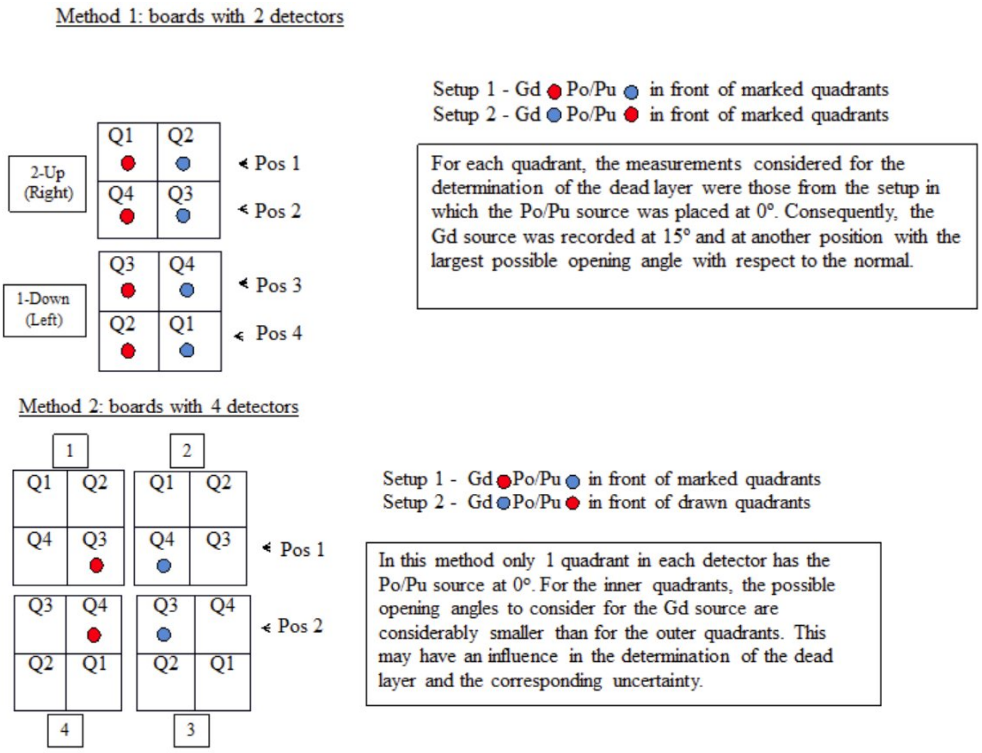

FIGURE 4.9: Schematic of α sources position and the subsequent methods used for calibration.

A mask was used (shown on fig. 4.5) to collimate the source allowing for a well defined angle of incidence, The drawing (see fig. 4.10) describes the effect of using a collimating mask and its importance in determining the angle when the α particles enter the detector, which determines the effective thickness of dead layer as seen by the incoming particle.

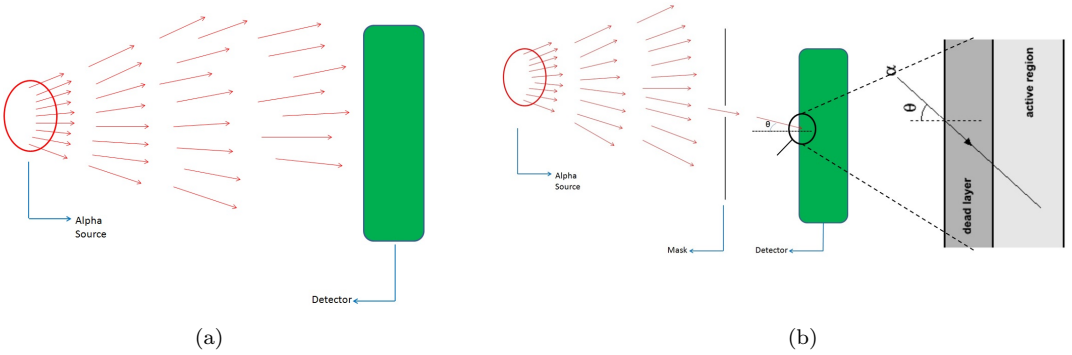

(a) (b)

FIGURE 4.10: Illustration of α particles travel from sources to detector without a collimator mask (a) and with mask (b).

The difference between added the collimator mask is specify the entry angle. For every measurement, made at a given relative position between the source and the masked quadrant, incident alpha particles impinged in a quadrant. In consequence, in different measurements we got different peaks in every quadrant due to different effective thickness of the traversed dead layer. The alpha sources are displaced parallel one another like in fig. 4.6, to have an 0° entry with the normal from the detector surface, in a specific quadrant. Taking this angle into account is fundamental because the statistic count are higher in this position and peaks have more resolution. We chose three measured positions which means 3 different angles of the incident particles, to estimate the dead layer thickness using the method explained in section 4.2.3. The other two positions were chosen properly in manner the finals results would give us an estimation near the expected thickness provided by manufacturer (∼0.8 μm).

From all detectors referenced before, part of them had connections troubles and even some of them were broken, on quadrants or even in all detecor. In total were no functioning 11 detectors plus 8 quadrants.

The vacuum inside the chamber during the calibrations was typically 10^{-7} mbar. Once this condition was achieved, detectors were biassed (-250V), controlling the leakage current increase, and the relative position between the sources and the masked detector was set properly. The movable stick (in particular translation up/down) where the alpha sources were fixed, allowed performing the whole set of measurements for a given board without opening the chamber, without breaking the vacuum and consequently saving considerable amount of time.

The used methods to differentiate the entry angle of particles on detector resulted on 3 chosen angles for all detectors in general. These 3 angles are equal for the same quadrants, any of detectors, in the method chosen. Lets see in detail the chosen angles for both methods and detectors quadrants in particular:

- Method 1 was initially used for boards of two detectors. The chosen angular positions of the sources specifically for each quadrant using this method were:

  Po/Pu at O° and Gd at 15° and 45° for Quadrants 1 and 2

  Po/Pu at O° and Gd at 15° and 37° for Quadrants 3 and 4

- Method 2 was considered for boards with 4 detectors. The chosen angular positions of the sources specifically for each quadrant using this method were:

  Po at 22° and Gd at 35° and 44° for Quadrant 1

  Po at 15° and Gd at 25° and 35° for Quadrant 2

  Po at 0° and Gd at 20° and 30° for Quadrant 3

  Po at 15° and Gd at 33° and 38° for Quadrant 4

During each measurement the data were stored in computer data files and we could observe the on-line spectra obtained for every quadrant. For the acquisition and the results viewing, we used an application called MIDAS [41], as mentioned in former sections. With this program the spectra could be visualized, and the time duration of each measurement controlled. For subsequent data analysis and estimation of the thickness of the dead-layer was used another program, ROOT [42], which makes easy to analyse the different peaks in every histogram.

4.2.2 Acquisition system and data analysis

In addition to processing the signal by means of the electronic chain, we also needs an acquisition system that allow us to digitise and store in a computer files data, for its subsequent analysis. The acquisition system chosen in this work was MIDAS (Multi Instance Data Acquisition System). The MIDAS software (the interface is represented on fig. 4.11) is based on a modular networking capable and central database system for data acquisition. It is a modular, object-based software system consisting of both Graphical User Interface and hardware control servers. It consists of a collection of C, C++ code handling the main functionality required for data communication between the different acquisition nodes, data control for run operation, data distribution for online data analysis among other capabilities. It provides the signal treatment from VMEbus, which allow us to represent in a histogram the output from ADC VME modules.

Data files stored with MIDAS have its own structure, which had to be converted to ROOT format files with a proper sorting code. The detailed analysis of the ROOT format data files was then performed with ROOT.

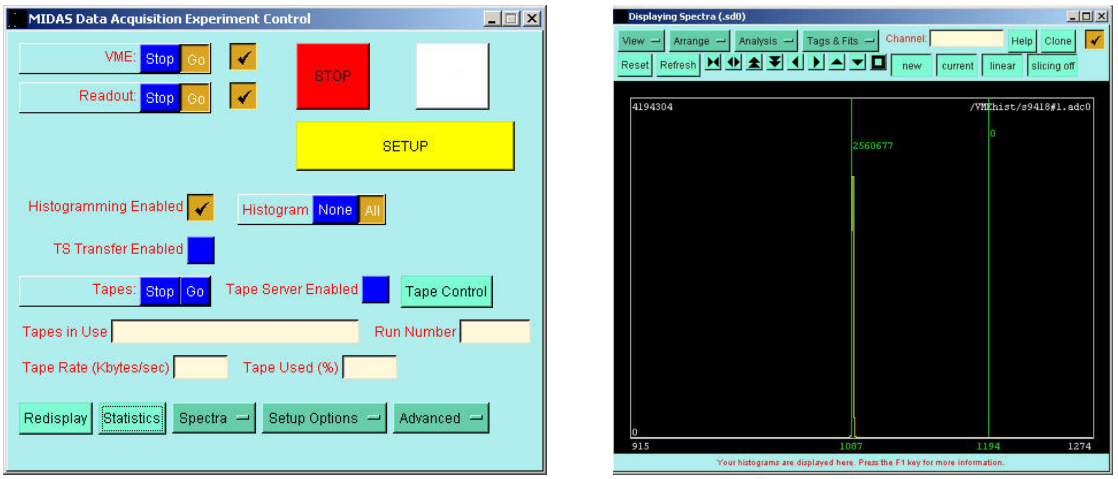

FIGURE 4.11: MIDAS interface. A typical histogram is shown on the right panel.

ROOT is an object-oriented program and library developed at CERN laboratories. It was originally designed for particle physics data analysis and contains several features specific to this field, but it is also used in other applications such as astronomy and data mining. ROOT is also a modular scientific software framework. It provides all the functionalities needed to deal with big data processing, statistical analysis, visualization and storage. It is mainly written in C++ but integrated with other languages such as Python and R. Starting from the ROOT format data files, we identify the ADC channel in the centroid of every peak on every histogram by fitting its distribution with a gaussian fit. The fig. 4.12 show us the ROOT interface as also one of the results obtained from the measures take place on CSIC, where it is seen 3 peaks corresponding to pulse, Gd and Po respectively.

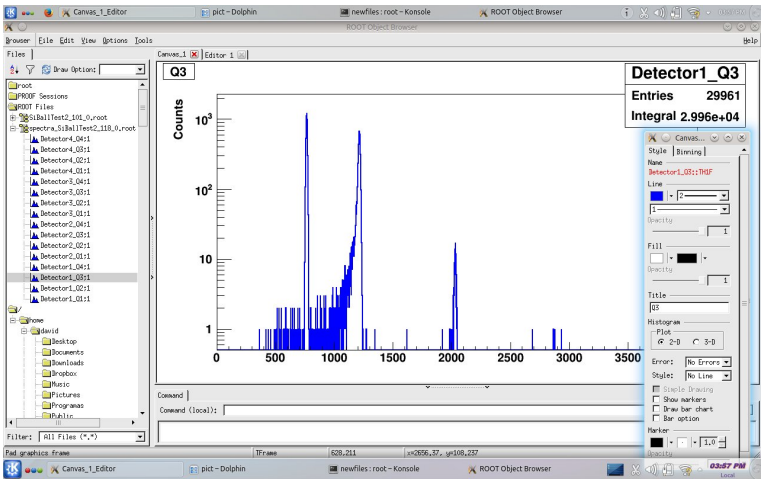

FIGURE 4.12: Root interface. Typical ADC channel histogram (that is, non energy calibrated) obtained for a quadrant detector (detector 1 quadrant 3 in the figure).

It was made an analysis to hundred of histograms and peaks included in them. Because of the dimension of data files and histograms it was developed a sorting code

to ROOT (see appendix A) in order to do it systematically and efficiently in terms of time. The results of all peak channel can be see in tables in appendix B.

The fig. 4.13 and fig. 4.14 show a plot of two measurements from different detectors. Both demonstrate their centroids to α particles emitted from each source, as well a fixed pulse which is inserted into the pre-amplifier to take the reply sub-control electronics chain. These figures represent the one-dimensional histograms of the ADC to a respective quadrant where the vertical axis indicates the counts in each ADC channel shown on the horizontal axis. It will be shown as example only two detector with characteristics results significantly different, not only with different methods and angles taken to measured but also from different boards. The spectra in red and blue on both figures represent two different positions of the alpha sources relative to the detector quadrant. It is perceptive the significant dead-layer thickness differences from each quadrant of same detectors for certain boards.

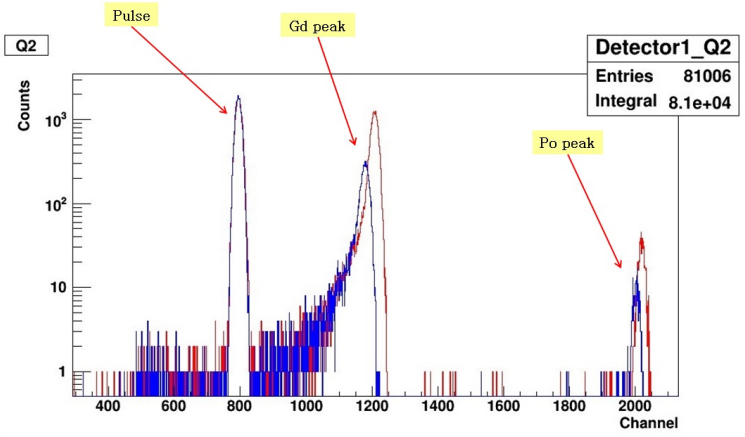

FIGURE 4.13: Spectra results of alpha particles detected from quadrant 2 of detector 1 of Board 1.

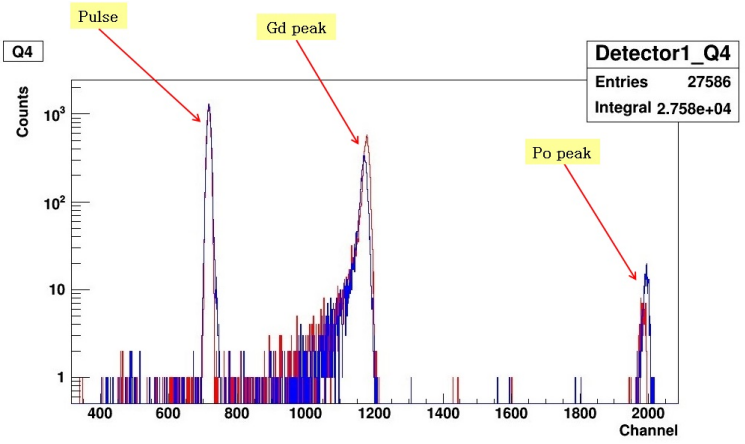

FIGURE 4.14: Spectra results of alpha particles detected from quadrant 4 of detector 1 of Board 11.

After the work developed on spectra program to calculate precisely the channels from peak sources, it is needed to calculate the energy loss of alpha ions in Silicon with an certain energy. Also we made a use of a SRIM tool (TRIM) to prove if the method which we are assuming for dead-layer thickness calculation, where we are assuming that the energy lost is constant along the material, it is no different of energy lost, where that energy is different every depth at which it passes through the material (this calculus is made in TRIM).

SRIM [43] is a software package concerning the Stopping and Range of Ions in Matter. SRIM is very popular in the ion implantation research and technology community and also used widely in other branches of radiation material science. SRIM is based on a Monte Carlo simulation method, namely the binary collision approximation with a random selection of the impact parameter of the next colliding ion. As the input parameters, it needs the ion type and energy (in the range 10 eV-2 GeV) and the material of one or several target layers. TRIM is a part of SRIM and treats the transport of ion in matter. TRIM will accept complex targets made of compound materials with up to eight layers, each of different materials. It will calculate both the final 3D distribution of the ions and also all kinetic phenomena associated with the ion's energy loss: target damage, sputtering, ionization, and phonon production. All target atom cascades in the target can be followed in detail.

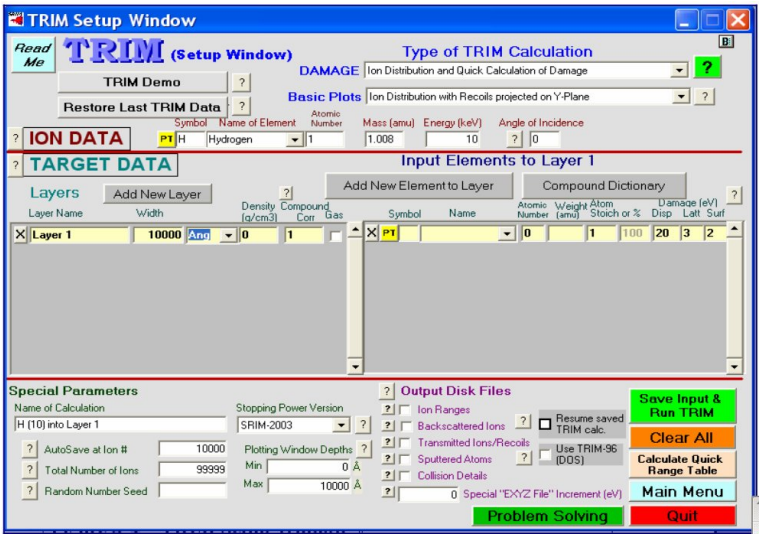

FIGURE 4.15: TRIM interface. Front pannel to study and calculate the stopping and range of ions [43].

Before passing to method of analysis it is important to compare the energy obtained in SRIM for a given peak, and the energy obtained by TRIM, where the transport is treated with a Monte Carlo simulation (MC TRIM). The fig. 4.16 shows the results of assuming a constant energy loss along the material for two different stopping powers at different depths, and the results obtain by TRIM in which the energy loss is not

constant in every depth that the charged particle passes through. In both cases there is no substantial difference between the MC TRIM and the constant energy loss per depth units up to 2 μm, well above the 0.8 μm expected from the manufacturer. Above 3 μm there is a slight deviation between both method.

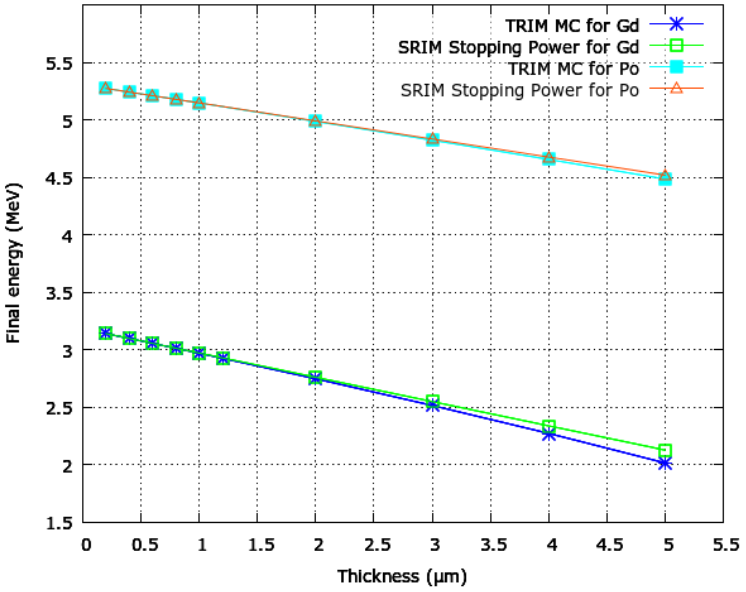

FIGURE 4.16: Trim method (Monte Carlo approximation) vs Experimental on different energies for different layer thickness.

4.2.3 Method for the analysis

The usual procedure to generating new energy calibrated histograms based on the original data files will briefly described in the following. In the new histograms, ADC channels registered on the original data files, noted as Ch, are converted into energy, E. The ADC channel to energy conversion is made through a linear function $E = a*Ch+b$, defined by its slope, a, and its intercept, b. The values of a and b depends upon two magnitudes:**i)** effective thickness of dead layer traversed by the alpha particles; **ii)** incident kinetic energy of the alpha particles.

To estimate the thickness of the dead-layer we use the equation (4.2). E_0 is the kinetic energy of the incident particle, $\frac{dE}{dx}$ is the energy lost of the particle in the dead layer, x is the thickness of the dead layer, θ is the angle formed by the velocity vector and the normal to the detector and E is the energy deposited in the active volume of Silicon, assuming that the detector is biassed so that it is fully depleted. The ratio $\frac{x}{\cos\theta}$ is the effective thickness of the dead layer for the angle of incident θ. In this work the stopping power $\frac{dE}{dx}$ (keV/μm) was calculated by means of SRIM. The stopping power is defined as the energy lost of a charged particle in a small length dx, and it is a magnitude

which depends upon the initial energy in general. When using the result obtained by SRIM, we assume that this magnitude is constant along the trajectory inside the depth layer.

$$E = E_0 - \frac{x}{\cos\theta}\frac{dE}{dx} \tag{4.2}$$

Replacing the energy of the left of the equation for the calibration in equation (4.3) we get the equation (4.4).

$$E(Ch) = aCh + b \tag{4.3}$$

$$aCh + b = E_0 - \frac{x}{\cos\theta}\frac{dE}{dx} \tag{4.4}$$

Where a, b and x are unknowns. To determine the thickness of the dead-layer of a quadrant we use a system of 3 equations with 3 unknowns variables. For every energy of the alpha particles emitted from the sources, three in total, we have three equations. An example could be a quadrant of the measurement where Po is at 0° with Ch_1, the Gd=15°, with Ch_2 and the Gd=46° with Ch_3, with the respective initial energy and stopping power, as shown below:

$$aCh_1 + b = E_0 - \frac{x}{\cos\theta_1}\frac{dE_1}{dx} \Rightarrow aCh_1 + b = 5304 - \frac{x}{\cos 0} * 1.837 * 10^2 \tag{4.5}$$

$$aCh_2 + b = E_0 - \frac{x}{\cos\theta_2}\frac{dE_2}{dx} \Rightarrow aCh_2 + b = 3182 - \frac{x}{\cos 15} * 1.39 * 10^2 \tag{4.6}$$

$$aCh_3 + b = E_0 - \frac{x}{\cos\theta_3}\frac{dE_3}{dx} \Rightarrow aCh_3 + b = 3182 - \frac{x}{\cos 46} * 1.837 * 10^2 \tag{4.7}$$

4.2.4 Experimental uncertainty

Every calculus has uncertainty associated for variables present on experiment, and for this experiment it is important to known the error of unknown thickness, just to have ensure the calculus were made correctively.

This lead us to know the experimental error a bit more. It is the difference between a measurement and the true value or between two measured values. Experimental error, itself, is measured by its accuracy and precision. Accuracy measures how close a measured value is to the true value or accepted value. Precision measures how closely two or more measurements agree with other.

Between accuracy and precision and how the angles were measured the accuracy is the systematic error that occurred, due of the unknown true value but close of the same.

Experimental errors, on the other hand, are inherent in the measurement process and cannot be eliminated simply by repeating the experiment no matter how carefully. There are two types of experimental errors: systematic errors and random errors.

Systematic errors are errors that affect the accuracy of a measurement. The accuracy of measurements subject to systematic errors cannot be improved by repeating those measurements. Common sources of systematic errors are faulty calibration of measuring instruments, poorly maintained instruments, or faulty reading of instruments by the user. A common form of this last source of systematic error is called "parallax error", which results from the user reading an instrument at an angle resulting in a reading which is consistently high or consistently low, which may be occur when reading distances between the source and the detector.

Random errors are errors that affect the precision of a measurement. Measurements subject to random errors differ from each other due to random, unpredictable variations in the measurement process.

Between accuracy and precision at how the angles were measured, the accuracy is the systematic error that occurred, due of the unknown true value but even close of the same. At the other hand for statistical measures of the energy deposited on detector converted to ADC channels the imprecision of the same is present, and the random errors make part of the experiment.

Propagation of error

In statistics, propagation of uncertainty (or propagation of error) is the effect of variables uncertainties (or errors, more specifically random errors) on the uncertainty of a function based on them. When the variables are the values of experimental measurements they have uncertainties due to measurement limitations (e.g., instrument precision) which propagate to the combination of variables in the function (4.8).

Neglecting correlations or assuming independent variables yields a common formula among engineers and experimental scientists to calculate error propagation, the variance formula.

$$s_f = \sqrt{(\frac{df}{dx})^2 s_x^2 + (\frac{df}{dy})^2 s_y^2 + (\frac{df}{dz})^2 s_z^2 + ...} \tag{4.8}$$

where s_f represents the standard deviation of the function f, s_x represents the standard deviation of x, s_y represents the standard deviation of y, and so forth.

The use of propagation of error equation was necessary to calculate the uncertainty associated to dead layer estimation for each quadrant. The program used to graphically demonstrate the results of the dead layer thickness used a theory of non-linear least-squares (NLLS) that generally is described in terms of a normal distribution of errors, which the input data is assumed to be a sample from a population having a given mean and a Gaussian (normal) distribution about the mean with a given standard deviation. At other hand it was used on mean and uncertainty calculus the weighted average method.

We conducted a preliminary estimation of the thickness of the dead-layer following the resolution given above. The obtained thicknesss are in the 0.7-0.9 μm range, which is compatible with thickness provided by the manufacturer ($\sim$0.8μm). The full results are provided and are described on next subsection 4.2.5.

4.2.5 Results

The conclusion of all results achieved after a long period of experiment done in CSIC are be presented below. To highlighting that all graphs and spectra are present on appendix C and only two of them will be shown, just to have in perspective the mainly differences between detectors and quadrants on the same detector, as the different methods the angular differences effects. Make reference too, besides only some of graphics be shown, the analyses of the calculations made for dead-layer thickness estimation from all detectors will be discussed in this subsection.

This results on dead-layer determination for all detector systems were tested more than multiple times and with different methods. The proven methods had the objective to made less differences of the thickness mean value from quadrants of same detector, i.e., to make possible the thickness of the 4 quadrants be close as it could be of the determined values.

In the following, the values of the dead-layer of the Si-Detectors of the Si-Ball system obtained from the measurements performed using Gd and Po/Pu sources are presented in gnuplot graphs from detector 1 Board 1 (fig. 4.17) and detector 1 Board 11 (fig. 4.18), and annexed for all other detectors tested. The gnuplot is a tool wich made possible to

draw graphically the values of dead-layer thickness with the respective error calculation 4.8, and also the mean value and the error of the dead-layer thickness.

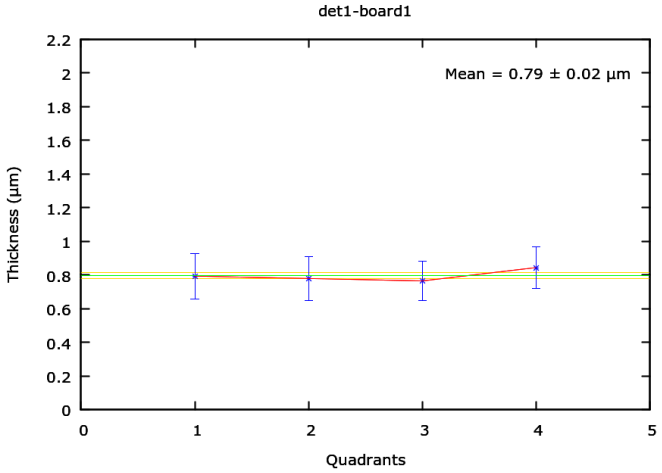

FIGURE 4.17: Results of dead-layer thickness for detector 1 from Board 1.

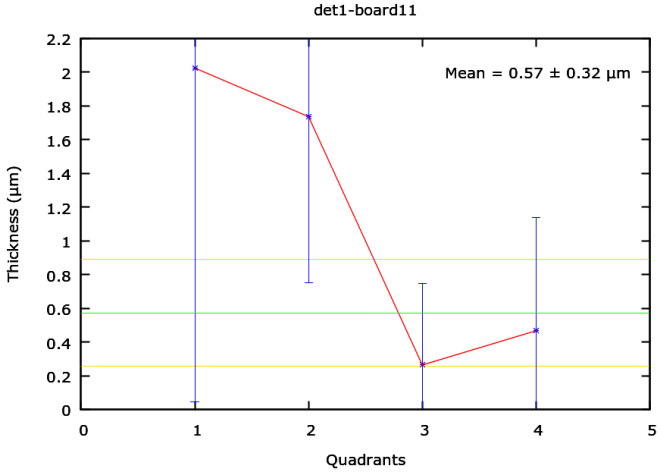

FIGURE 4.18: Results of dead-layer thickness for detector 1 from Board 11.

The dead-layer values obtained for the studied detectors are presented. In each graph, the result of the dead-layer of all quadrants is presented with its corresponding uncertainty. The green line represents the result of the fit of a constant function to all data points. The gold line shows the uncertainty resulting from the fit. These numbers are not always close to the mean values and their uncertainties for the dead-layer of the detectors presented in the table beneath.

The graphs summarizing the results are followed by tables 4.2 for 2 detector Boards and 4.3 for 4 detector Boards, with the derived values and a description of the methods considered (explained in subsection 4.2.1) for each kind of board. The tables show us all quadrant and detectors operative from which Board, as the correspondent dead-layer thickness, it's mean value for all detector and the associated error and the method used

to calculate it. Comments on the possible origin of the discrepancies are given post this visualization.

TABLE 4.2: Dead-layer values from boards with 2 detectors

		Board with 2 detectors (thickness)					
		QUADRANTS					
Board	**Detector**	**Q1** (μm)	**Q2** (μm)	**Q3** (μm)	**Q4** (μm)	**Mean** (μm)	**Method**
1	1	0.793±0.134	0.779±0.132	0.764±0.118	0.843±0.125	**0.79±0.06**	1
	2	0.639±0.111	0.600±0.105	0.563±0.104	0.594±0.106	**0.60±0.05**	1
2	1		0.695±0.119	0.787±0.121	0.854±0.126	**0.78±0.07**	1
3	1		0.690±0.118	0.624±0.106	0.747±0.116	**0.68±0.07**	1
	2	0.716±0.123	0.662±0.115	0.568±0.104		**0.64±0.07**	1
6	1	0.661±0.169	1.246±0.282	1.705±0.481	0.996±0.322	**0.9±0.1**	2
	2	0.878±0.210	0.472±0.141	0.184±0.214	0.428±0.234	**0.49±0.09**	2
7	2	0.922±0.218	0.941±0.224	1.037±0.336	0.967±0.321	**1.0±0.1**	2
8	2	0.827±0.139	0.659±0.114	0.520±0.101	0.853±0.128	**0.68±0.06**	1

TABLE 4.3: Dead-layer values from boards with 4 detectors

		Board with 4 detectors (thickness)					
		QUADRANTS					
Board	**Detector**	**Q1** (μm)	**Q2** (μm)	**Q3** (μm)	**Q4** (μm)	**Mean** (μm)	**Method**
9	1		1.179±0.214	1.475±0.425	1.358±0.624	**1.2±0.2**	2
	2	0.961±0.184	0.958±0.250	0.890±0.444	0.945±0.316	**0.9±0.1**	2
	3	0.856±0.227	0.909±0.178	0.776±0.284	0.552±0.328	**0.8±0.1**	2
	4		0.902±0.235	0.511±0.322	0.833±0.293	**0.8±0.2**	2
10	1	1.138±0.286	1.154±0.210	1.440±0.416	0.858±0.427	**1.2±0.2**	2
	2	1.115±0.205	1.210±0.305	1.657±0.754	1.607±0.454	**1.2±0.2**	2
11	1	2.024±1.978	1.736±0.983	0.263±0.482	0.466±0.673	**0.6±0.4**	2
	2	1.276±0.794	1.919±1.888	0.202±0.567	0.318±0.504	**0.5±0.3**	2
12	1	0.849±0.223	0.886±0.172	0.797±0.289	0.460±0.298	**0.8±0.1**	2
	2	0.871±0.171	0.889±0.234	0.696±0.375	0.782±0.286	**0.8±0.1**	2
	3	1.040±0.266	1.239±0.225	1.389±0.404	1.128±0.531	**1.2±0.2**	2
	4	1.152±0.211	1.185±0.297	1.477±0.677	1.302±0.387	**1.2±0.2**	2
E	1	0.841±0.221	0.940±0.179	0.221±0.214	0.812±0.424	**0.7±0.1**	2
	2	0.980±0.186	0.806±0.217	0.486±0.311	0.706±0.274	**0.8±0.1**	2
	3			1.703±0.476	1.421±0.652	**1.6±0.4**	2
	4	1.106±0.205		1.007±0.487	1.184±0.364	**1.1±0.2**	2

Discussion:

As we can observe, the obtained values of the dead-layer of the detectors varies between 0.49 and 1.56 μm, with errors ranging between a few percent to 34%. In my opinion, this large spread is due to the different methods used in the calibration, which in some cases for certain quadrants may turn into a wrong determination of the dead-layer. With the goal of determining the origin of this large spread and the possible nature of the large errors in some of the measurements, we start by analysing the chronological sequence in which the various boards were exposed to the sources. The sequence is: 3 8 2 1 9 10 E 12 7 6 11 (board number).

Up to the measurement of board number 1, the method used (1) consisted in locating the sources in front of all quadrants. After board number 9, the method considered (2) only positioned the source in front of some of the quadrants (not all). This difference between the methods does clearly have an impact on the results, as the mean values of the dead-layer obtained for detectors in boards 3, 8, 2 and 1, vary between 0,6 and 0,8 μm, with typical errors below 10%. On the contrary, the dead-layer value obtained for the rest of the boards using Method 2 present a large spread (from 0.49 to 1.56 μm), with errors ranging from 15% up to 40%.

As we can see, the smaller difference in angular position for the Gd-source on Quadrants 3 and 4 translates into slightly larger deviations in the obtained dead-layer value for these quadrants.

In basically all cases, the angular opening (the angular difference between both measurements) for the Gd runs is considerably smaller than method 1, which can induce to possible deviations in the calculation of the dead-layer. For board 7 and 6 we only use 2 positions (2 and 3) with low angular difference as well, and for board 11 position 1 (method 2) and a new position 0 with sources in front of Q2 detector 1 and Q1 detector 2. A preliminary conclusion can be that method 1 provides consistent values for all quadrants of the investigated detectors, resulting in a mean value in agreement with the specifications given by the manufacturer. This does not apply to the detectors for which the dead-layer was measured using the method 2. The main difference between the methods is the angular opening for the measurements on the Gd source. When considering in the analysis runs with an angular opening lower that 20° (as it is the case in Method 2), inconsistencies start to appear. Even within this method, the positions considered for Quadrants 1 and 2 result in consistent results, whereas the values obtained for Quadrants 3 and 4 deviate considerably. Overall we can conclude that the angular difference between the Gd source measurements can be pointed as a first source of error in the determination of some of the dead-layer of the detectors, indicating an eventually need of repeating the measurements using method 1.

Chapter 5

Summary and conclusions

This chapter is devoted to quote the works done in the framework of the present master thesis, described in the previous chapters, to highlight the main conclusions and to point out future works that may be subsequently addressed.

The present master thesis was carried out based in the work done in three institutions: CSIC, CMAM, UCM (Madrid, Spain) and University of Lisbon (Portugal). The aim of the work was to measure the thickness of the dead layer of the set of Silicon detectors which forms the Silicon Ball array. A dedicated test bench was assembled and put at work in order to perform the needed experimental measurements.

The setting up of the test bench and the measurements were performed in Madrid during a six months stay of the author that was possible thanks to the ERASMUS program. Most of the analysis of the experimental data and its interpretation was carried out in the Faculdade de Ciências of the University of Lisbon.

I spent several weeks getting a general view of accelerator technology, vacuum systems and specially nuclear instrumentation used in experimental studies performed at CMAM and Instituto de Estructura de la Materia-CSIC. I learn to work with scientific applications that was planned to use at different stages of the work as MIDAS, ROOT, SRIM/TRIM and gnuplot.

Guided by experts from the research groups CSIC, and professor Luis Mario from UCM/UAM, I mounted and put at work a fully equipped test bench to carry out the set of measurements, which consisted of irradiating with alpha particles every Silicon detector of the Si-ball array under controlled conditions. In particular, special attention was paid for collimating the alpha particles emitted by the sources in order to get the required accuracy for the incidence angle.

The collected computer data files, in MIDAS format, were converted to ROOT format. Within the ROOT framework, I implemented a sorting code for analyzing in a systematic and automated way the peaks in the ADC histograms due to the emitted alpha particles. It must be notice that the set of detectors (also referred as quadrants in the text) and alpha particle sources results in more than a hundred peaks to be analyzed. Among other relevant quantities obtained from the fit of every peak, the centroid plays a central role in the methodology followed for experimentally evaluating the thickness of the dear layer.

For the energy calibration of every detector it was taken into account the following parameters: **i)** thickness of its dead layer, to be calculated as a side product of the calibration procedure; **ii)** incidence angle of the alpha particle; **iii)** tabulated stopping power for alpha particles in aluminum calculated by SRIM at relevant energies. Considering the nominal thickness of the dead layer given by the manufacturer, of the order of micrometers, and the well known energy dependence of the stopping power (Bragg curve), it was used an energy independent stopping power for the calibration procedure.

TRIM Monte Carlo simulations for alpha particles in aluminum at relevant energies were performed, to be compared with those obtained under the approximation of SRIM energy independent stopping power. It was found that the results given by TRIM and SRIM on the energy deposition of the alpha particles emitted by the used alpha sources are practically the same up to 3 micrometers. This result supports the energy independent stopping power approximation that was used for the experimental evaluation of the thickness of the dead layer.

The analysis of death layer thickness from Si-ball detectors had different results essentially on experimental method picked to chose the entry angles from detector normal surface with the incident α particles. Was observed an enormous variance of both methods results. We used two methods that could provides the exactly angular approximation we needed and enough energy resolution to detect the α particles. After the results observation it was concluded that the difference between the methods does clearly have an impact on the results, as the mean values of the dead-layer obtained for detectors in boards. The obtained experimental values of the dead layer thickness of the Si-ball detectors vary in a wide range, from 0.49 μm up to 1.6 μm. The nominal value given by manufacturer is 0.8 μm.

The dead layer thickness in Si-ball detectors reveals as a crucial element for scattering experiments where high energy resolution for reaction fragments (ie: proton, deuteron, triton, alpha, etc.) must be achieved. In this work we show that special attention must be paid to the kinematics of the reaction since the energy resolution within one quadrant can be spoiled due to the influence of the effective thickness of the dead layer.

A detailed study for a selected set of reactions about the interplay of the effective dead layer thickness of every Si-ball detector and the beam characteristics on the scattering target (size, divergence, etc.) would be helpful in order to estimate the performances of Si-ball in such cases. This studies could be addressed by means of realistic Monte Carlo simulations which can be done with Geant4 tool.

Acknowledgements

At first place I would like to thank to my supervisors, Daniel Galaviz Redondo and Ángel Miguel Sánchez Benitez for giving me the opportunity to present this thesis and take part of this experience as the all support and knowledge transmitted.

I would also want to thank to professor Luis Mario Fraile Prieto to have given me all the help, support and learning while I stayed in Madrid. Also thank to all physics team collaborators from Complutense University of Madrid to the time spent together, the lunch time, and the appreciation that had to receive me. A special thank to Mariano Carmona Gallardo for the laughs and the help given to me, to Francisco Javier Ulla Pedrera to the work developed together on mounting the test bench for Si-ball. Give thanks to CSIC collaborators on the assistance provided. Another special thank to Pamela who provided an enormous help in this final stage of my thesis.

A final thank to my family and friends for the support and friendship. THANK YOU.

Appendices

Appendix A

ROOT sorting code

In the following are represented the ROOT code used for the peak channel finder for the correspondent α particles.

```
void FitSinglePeak(TH1F *hist, Double_t X_LO, Double_t X_HI)
{

//   gStyle->SetFitFormat("8.6g");

 if(X_LO < X_HI)
  {
   TF1* fitfunc = new TF1("gauss_linbg",gaus_lbg, X_LO, X_HI, 5);
   gBinW= hist->GetBinWidth(1);
   fitfunc->SetParNames("BgConstant","BgSlope","Sigma", "Area","Position");
   fitfunc->SetParameters(0,0,0.3*(X_HI-X_LO),
   hist->Integral(hist->FindBin(X_LO),hist->FindBin(X_HI)),0.5*(X_LO+X_HI));
   fitfunc->SetParLimits(3,0,1e7);
   fitfunc->SetParLimits(2,0,100);

   hist->Fit(fitfunc,"QRM");

  TF1 *LineaRecta = new TF1("LineaRecta","pol1", X_LO,X_HI );
  LineaRecta->SetParameter(0,  fitfunc->GetParameter(0)  );
  LineaRecta->SetParameter(1,  fitfunc->GetParameter(1)  );
  LineaRecta->SetLineColor(kGreen);
  TF1 *Gauss1= new TF1("Gauss1",gaus_lbg, X_LO,X_HI,5 );
  Gauss1->SetParameter(0,  fitfunc->GetParameter(0)  );
  Gauss1->SetParameter(1,  fitfunc->GetParameter(1)  );
  Gauss1->SetParameter(2,  fitfunc->GetParameter(2)  );
  Gauss1->SetParameter(3,  fitfunc->GetParameter(3)  );
  Gauss1->SetParameter(4,  fitfunc->GetParameter(4)  );

  Gauss1->SetLineColor(kBlue);
  LineaRecta->Draw("same");
  Gauss1->Draw("same");
```

```
   printf("\tChi Square: %f\n",fitfunc->GetChisquare());
   printf("\t      FWHM: %f +- %f\n",2*fitfunc->GetParameter(2)*sqrt(2*log(2)),
   2*sqrt(2*log(2))*fitfunc->GetParError(2));

   printf("%f  %f  %f  %f  %f  %f\n",fitfunc->GetParameter(4),fitfunc->GetParError(4),
   fitfunc->GetParameter(3),fitfunc->GetParError(3),
   fitfunc-> GetParameter(2),fitfunc->GetParError(2));
   printf("\tPosition: %f +- %f\n",fitfunc->GetParameter(4),fitfunc->GetParError(4));
   printf("\tArea: %f +- %f\n",fitfunc->GetParameter(3),fitfunc->GetParError(3));
   printf("\tSigma: %f +- %f\n",fitfunc->GetParameter(2),fitfunc->GetParError(2));

  } else cout << "Couldn't fit! Error: The Lower Limit is larger
   than the Upper Limit!" << endl;
}
```

Or if we want to find 2 peaks at once.

```
void FitSinglePeakbckg(TH1F *hist, Double_t X_left_1, Double_t X_left_2,
Double_t X_LO, Double_t X_HI, Double_t X_right_1, Double_t X_right_2)
{
//   gStyle->SetFitFormat("8.6g");

 if(X_LO < X_HI)
  {
   TF1* fitfunc = new TF1("gauss_linbg",gaus_lbg, X_left_1, X_right_2, 5);
   gBinW= hist->GetBinWidth(1);

   Double_t xleft1=hist->FindBin(X_left_1);
   Double_t xleft2=hist->FindBin(X_left_2);

   Double_t xright1=hist->FindBin(X_right_1);
   Double_t xright2=hist->FindBin(X_right_2);

   Double_t a[35000],b[35000];

   Int_t j=0;
   for (Int_t i=xleft1; i<xleft2+1;i++) {
        a[j]=gBinW*(i+0.5);
        b[j]=hist->GetBinContent(i);
        j++;
   }

   for(Int_t i=xright1; i<xright2+1;i++){
        a[j]=gBinW*(i+0.5);
        b[j]=hist->GetBinContent(i);
        j++;
   }

  Int_t maxdim,mindim,rdim;
  maxdim=j;

  Double_t* c = new Double_t[maxdim];
  Double_t* d = new Double_t[maxdim];
  cout<<"maxdim "<<maxdim<<" mindim "<<mindim<<" rdim "<<rdim<<endl;

  Int_t n=0;
  for(i=0 ; i<maxdim ; i++ ){
    c[n]=a[i];
    d[n]=b[i];
       cout<<"a "<<i<<" = "<<a[i]<<" y b = "<<b[i]<<" c "<<n<<" =
        "<<c[n]<<" y d = "<<d[n]<<" n "<<n<<   endl;
   n++;
}

  TGraph* graph = new TGraph(maxdim,c,d);
//
  TF1 *LineaRecta = new TF1("LineaRecta","pol1", X_left_1,X_right_2);
  LineaRecta->SetParameter(0,  100.  );
  LineaRecta->SetParameter(1,  -0.001 );
```

```
  cout << "empezamos a fitear linearecta" << endl;
 graph->SetMarkerStyle(21);
 graph->SetMarkerSize(0.7);
  graph->Fit(LineaRecta,"");
//    ,"",X_left_1,X_right_2
    cout << "terminamos de fitear linearecta" << endl;
  LineaRecta->SetLineColor(kGreen);

  hist->SetLineColor(kBlue);
  hist->Draw();
//      graph->Draw("ap");


  fitfunc->SetParNames( "BgConstant", "BgSlope", "Sigma", "Area", "Position");
   fitfunc->SetParameters(0, 0, 0.3*(X_HI-X_LO), hist->Integral(hist->FindBin(X_LO),
   hist->FindBin(X_HI)), 0.5*(X_LO+X_HI));


   fitfunc->FixParameter(0,LineaRecta->GetParameter(0));
   fitfunc->FixParameter(1,LineaRecta->GetParameter(1));
   fitfunc->SetParLimits(4,X_LO,X_HI);
//    fitfunc->SetParLimits(2,0.,(X_HI-X_LO)/2.);
   fitfunc->SetParLimits(2,0.,250);
   fitfunc->SetLineColor(kBlue);
   hist->Fit(fitfunc,"QRM");

//   TF1 *Gauss1= new TF1("Gauss1","gaus", X_LO,X_HI );
//   Gauss1->SetParameter(0,  fitfunc->GetParameter(2)  );
//   Gauss1->SetParameter(1,  fitfunc->GetParameter(3)  );
//   Gauss1->SetParameter(2,  fitfunc->GetParameter(4)  );
//   Gauss1->SetLineColor(kBlue);

//   TF1 *Gauss2= new TF1("Gauss2","gaus", X_LO,X_HI );
//   Gauss2->SetParameter(0,  fitfunc->GetParameter(5)  );
//   Gauss2->SetParameter(1,  fitfunc->GetParameter(6)  );
//   Gauss2->SetParameter(2,  fitfunc->GetParameter(7)  );
//   Gauss2->SetLineColor(kRed);

//   Gauss1->Draw("same");
//   Gauss2->Draw("same");

//   TF1* total1 = new TF1("total1","pol1(0)+gaus(2)",X_left_1,X_right_2,5);
// total2 = new TF1("total2",LineaRecta+Gauss2, X_LO,X_HI);
//   total1->SetLineColor(kBlue);

  //   total2->SetLineColor(kRed);

//   total1->Draw("same");
    LineaRecta->Draw("same");
// total2->Draw("same");

   //    RMIEL
/*   printf("\tChi Square: %f\n",fitfunc->GetChisquare());
   printf("\t       FWHM: %f +- %f\n",2*fitfunc->GetParameter(2)*sqrt(2*log(2)),
   2*sqrt(2*log(2))*fitfunc->GetParError(2));
```

```
  */
   printf("%f  %f  %f  %f  %f  %f\n",fitfunc->GetParameter(4),fitfunc->GetParError(4),
   fitfunc->GetParameter(3),fitfunc->GetParError(3),fitfunc->
   GetParameter(2),fitfunc->GetParError(2));
   printf("\tPosition: %f +- %f\n",fitfunc->GetParameter(4),fitfunc->GetParError(4));
   printf("\tArea: %f +- %f\n",fitfunc->GetParameter(3),fitfunc->GetParError(3));
   printf("\tSigma: %f +- %f\n",fitfunc->GetParameter(2),fitfunc->GetParError(2));

  } else cout << "Couldn't fit! Error: The Lower Limit is larger
  than the Upper Limit!" << endl;
}
```

Appendix B

Peak channels from alpha sources

In the following are represented the the peak channel for the correspondent α particles in ROOT program. Each line correspond to a run done at a determine position

TABLE B.1: Peak channels from ROOT spectra for boards with 2 detectors.

	Detector 2								Detector 1							
	Q4		Q3		Q2		Q1		Q4		Q3		Q2		Q1	
	^{148}Gd	^{210}Po	^{148}Gd	^{210}Po	^{148}Gd	^{210}Po	^{148}Gd	^{210}Po	^{148}Gd	^{210}Po	^{148}Gd	^{210}Po	^{148}Gd	^{210}Po	^{148}Gd	^{210}Po
Board #1	1143	1941	1139	1932	1119	1885	1171	1967	1161	1987	1177	1995	1175	2002	1146	1973
	1148	1942	1145	1934	1119	1884	1170	1965	1171	1993	1191	1999	1191	2009	1159	1981
	1147	1942	1141	1932	1109	1878	1161	1960	1181	1997	1199	2005	1205	2016	1173	1987
	1139	1936	1133	1928	1100	1872	1147	1953	1175	1994	1196	2002	1208	2020	1176	1991
	1148	1946	1147	1934	1121	1875	1177	1968	1169	1990	1200	2018	1185	2012	1158	1974
	1152	1946	1147	1934	1117	1876	1172	1968	1176	1993	1223	2028	1194	2018	1163	1984
	1147	1942	1145	1934	1108	1868	1166	1966	1184	1997	1212	2029	1209	2020	1175	1987
	1142	1938	1140	1924	1101	1863	1155	1955	1182	1995	1213	2029	1209	2025	1181	1984
Board #2	-	-	-	-	-	-	-	-	1156	1981	1172	2000	1186	2005	-	-
	-	-	-	-	-	-	-	-	1166	1988	1187	2006	1195	2011	-	-
	-	-	-	-	-	-	-	-	1169	1991	1198	2015	1205	2013	-	-
	-	-	-	-	-	-	-	-	1168	1989	1199	2016	1198	2014	-	-
	-	-	-	-	-	-	-	-	1162	1979	1181	2004	1175	1999	-	-
	-	-	-	-	-	-	-	-	1171	1983	1192	2008	1186	2006	-	-
	-	-	-	-	-	-	-	-	1175	1986	1199	2012	1198	2012	-	-
	-	-	-	-	-	-	-	-	1174	1987	1184	1988	1201	2012	-	-
Board #3	-	-	1145	1880	1157	1891	1176	1910	1160	1925	1204	1971	1185	1947	-	-
	-	-	1146	1880	1155	1889	1174	1911	1168	1930	1211	1977	1195	1958	-	-
	-	-	1143	1879	1144	1882	1165	1902	1174	1935	1217	1973	1208	1962	-	-
	-	-	1135	1871	1137	1875	1154	1895	1173	1934	1215	1974	1212	1963	-	-
	-	-	1151	1880	1170	1895	1176	1913	1170	1929	1202	1973	1183	1954	-	-
	-	-	1151	1879	1163	1891	1171	1911	1174	1931	1208	1976	1191	1956	-	-
	-	-	1146	1875	1152	1887	1163	1905	1180	1933	1214	1972	1205	1961	-	-
	-	-	1143	1872	1143	1883	1154	1899	1182	1927	1213	1971	1207	1965	-	-
Board #6	1145	1942	1140	1932	1118	1888	1169	1964	1161	1984	1176	1982	1180	1995	1149	1971
	1144	1941	1137	1930	1110	1884	1159	1959	1170	1988	1183	1987	1191	2003	1162	1978
	1144	1943	1144	1929	1126	1888	1170	1967	1164	1980	1176	1987	1176	1993	1150	1966
	1142	1940	1140	1927	1114	1880	1158	1957	1176	1987	1187	1994	1195	2009	1172	1979
Board #7	1145	1945	1132	1930	1108	1884	1164	1962	1175	1983	1213	2031	1201	2011	1160	1962
	1144	1945	1131	1931	1113	1886	1167	1963	1173	1984	1211	2031	1205	2013	1165	1964
	1148	1942	1139	1924	1115	1876	1172	1963	1169	1992	1206	2028	1205	2020	1168	1985
	1151	1943	1143	1925	1116	1873	1170	1961	1168	1992	1207	2030	1201	2018	1163	1983
Board #8	1149	1944	1147	1937	1158	1946	1176	1968	-	-	-	-	-	-	-	-
	1152	1944	1148	1937	1152	1941	1174	1963	-	-	-	-	-	-	-	-
	1159	1944	1146	1935	1146	1939	1163	1961	-	-	-	-	-	-	-	-
	1142	1940	1139	1934	1135	1935	1151	1956	-	-	-	-	-	-	-	-
	1148	1945	1151	1933	1118	1869	1171	1968	-	-	-	-	-	-	-	-
	1150	1946	1152	1933	1115	1867	1169	1965	-	-	-	-	-	-	-	-
	1141	1943	1145	1931	1103	1863	1157	1961	-	-	-	-	-	-	-	-
	1135	1938	1137	1926	1092	1856	1147	1954	-	-	-	-	-	-	-	-

TABLE B.2: Peak channels from ROOT spectra for boards with 4 detectors.

	Detector 4								Detector 3								Detector 2								Detector 1							
	Q4		Q3		Q2		Q1		Q4		Q3		Q2		Q1		Q4		Q3		Q2		Q1		Q4		Q3		Q2		Q1	
	^{148}Gd	^{209}Po	^{148}Gd	^{209}Po	^{148}Gd	^{209}Po	^{148}Gd	^{209}Po	^{148}Gd	^{209}Po	^{148}Gd	^{209}Po	^{148}Gd	^{209}Po	^{148}Gd	^{209}Po	^{148}Gd	^{209}Po	^{148}Gd	^{209}Po	^{148}Gd	^{209}Po	^{148}Gd	^{209}Po	^{148}Gd	^{209}Po	^{148}Gd	^{209}Po	^{148}Gd	^{209}Po
Board #9	1175	1989	1125	1906	1147	1949	break	break	1150	1964	1150	1974	1110	1900	1093	1885	1141	1943	1226	1926	1084	1848	1162	1963	1177	1984	1157	1936	1202	2013	break	break
	1181	1992	1130	1908	1162	1956	break	break	1156	1969	1165	1978	1124	1910	1105	1895	1135	1936	1221	1921	1073	1840	1150	1954	1168	1978	1149	1931	1184	2003	break	break
	1174	1990	1102	1887	1141	1956	break	break	1161	1957	1166	1970	1116	1896	1104	1879	1146	1938	1136	1916	1076	1811	1167	1959	1169	1990	1181	1982	1198	2016	break	break
	1179	1994	1105	1891	1151	1964	break	break	1167	1960	1172	1973	1132	1904	1117	1887	1138	1934	1227	1913	1062	1807	1150	1951	1158	1984	1170	1977	1180	2004	break	break
Board #10	BAD PEAK	BAD PEAK	BAD PEAK	BAD PEAK	BAD PEAK	BAD PEAK	BAD PEAK	BAD PEAK	BAD PEAK	BAD PEAK	BAD PEAK	BAD PEAK	BAD PEAK	BAD PEAK	BAD PEAK	BAD PEAK	1139	1940	1222	1923	1089	1868	1152	1956	1169	1976	1170	1963	1170	1974	1148	1954
	BAD PEAK	BAD PEAK	BAD PEAK	BAD PEAK	BAD PEAK	BAD PEAK	BAD PEAK	BAD PEAK	BAD PEAK	BAD PEAK	BAD PEAK	BAD PEAK	BAD PEAK	BAD PEAK	BAD PEAK	BAD PEAK	1151	1940	1144	1920	1117	1869	1174	1963	1163	1992	1185	1991	1194	2009	1157	1980
	BAD PEAK	BAD PEAK	BAD PEAK	BAD PEAK	BAD PEAK	BAD PEAK	BAD PEAK	BAD PEAK	BAD PEAK	BAD PEAK	BAD PEAK	BAD PEAK	BAD PEAK	BAD PEAK	BAD PEAK	BAD PEAK	1142	1934	1137	1916	1102	1861	1157	1952	1156	1985	1176	1984	1177	1995	1141	1966
	BAD PEAK	BAD PEAK	BAD PEAK	BAD PEAK	BAD PEAK	BAD PEAK	BAD PEAK	BAD PEAK	BAD PEAK	BAD PEAK	BAD PEAK	BAD PEAK	BAD PEAK	BAD PEAK	BAD PEAK	BAD PEAK	1147	1950	1131	1934	1106	1881	1168	1971	1176	1981	1164	1942	1198	2005	1167	1973
Board #11	BAD PEAK	BAD PEAK	BAD PEAK	BAD PEAK	BAD PEAK	BAD PEAK	BAD PEAK	BAD PEAK	break	break	break	break	break	break	break	break	1145	1945	1132	1930	1108	1884	1164	1962	1175	1983	1213	2031	1201	2011	1160	1962
	BAD PEAK	BAD PEAK	BAD PEAK	BAD PEAK	BAD PEAK	BAD PEAK	BAD PEAK	BAD PEAK	break	break	break	break	break	break	break	break	1144	1945	1131	1931	1133	1886	1167	1963	1173	1984	1211	2031	1205	2013	1165	1964
	BAD PEAK	BAD PEAK	BAD PEAK	BAD PEAK	BAD PEAK	BAD PEAK	BAD PEAK	BAD PEAK	break	break	break	break	break	break	break	break	1148	1942	1139	1924	1115	1876	1172	1963	1169	1992	1206	2028	1205	2020	1168	1985
	BAD PEAK	BAD PEAK	BAD PEAK	BAD PEAK	BAD PEAK	BAD PEAK	BAD PEAK	BAD PEAK	break	break	break	break	break	break	break	break	1151	1943	1143	1925	1116	1873	1170	1961	1168	1992	1207	2030	1201	2018	1163	1983
Board #12	1152	1956	1126	1916	1141	1950	1123	1923	1144	1965	1154	1974	1107	1899	1088	1887	1136	1942	1119	1926	1098	1877	1160	1965	1174	1983	1166	1955	1198	2007	1168	1971
	1165	1961	1138	1922	1163	1962	1143	1933	1153	1970	1164	1981	1122	1911	1102	1895	1130	1938	1114	1922	1086	1870	1145	1955	1170	1978	1171	1967	1181	1996	1153	1961
	1153	1960	1119	1922	1136	1957	1126	1923	1165	1959	1166	1972	1116	1896	1106	1880	1148	1939	1140	1921	1114	1870	1170	1961	1162	1990	1180	1985	1194	2008	1155	1977
	1163	1967	1126	1928	1153	1968	1143	1933	1172	1963	1174	1976	1132	1906	1121	1889	1141	1935	1134	1918	1102	1865	1155	1952	1158	1985	1175	1981	1180	1999	1144	1969
Board #E	1130	1926	1127	1909	1142	1886 (badp)	1127	1916	1151	1963	1160	1972	break	break	break	break	1143	1943	1126	1928	1112	1898	1163	1964	1176	1980	1174	1963	1198	2003	1163	1965
	1148	1932	1135	1914	1160	no peak	1144	1928	1159	1972	1169	1979	break	break	1110	1898	1138	1939	1123	1924	1102	1890	1148	1954	1170	1978	1170	1962	1183	1994	1132	1932
	1138	1936	1119	1923	1130	1942	1123	1923	1164	1958	1164	1972	break	break	break	break	1140	1943	1140	1921	1135	1908	1170	1963	1163	1992	1188	2001	1195	2014	1155	1981
	1142	1938	1122	1925	1141	1952	1130	1932	1172	1962	1174	1976	break	break	1122	1891	1142	1937	1134	1916	1120	1898	1155	1952	1157	1987	1185	2002	1180	2004	1143	1973

Appendix C

Dead layer thickness results

In the following are represented the dead-layer thickness results for the remaining detectors analyzed.

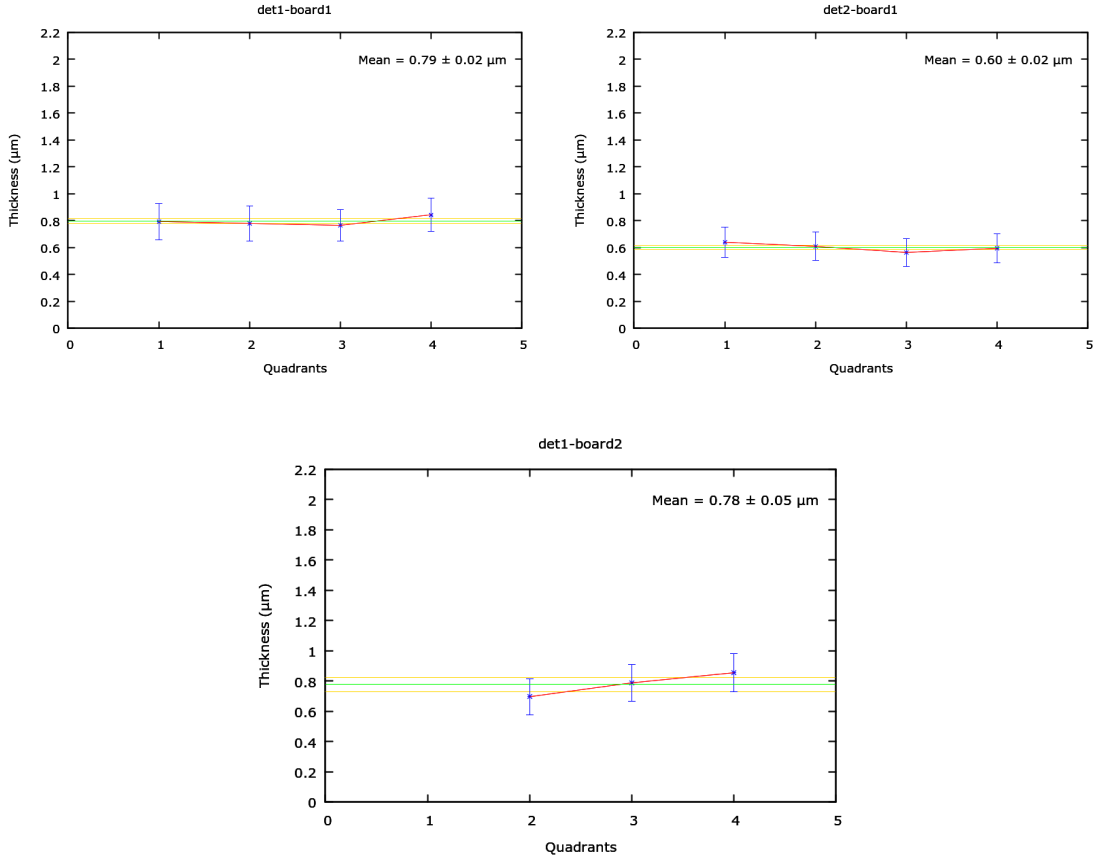

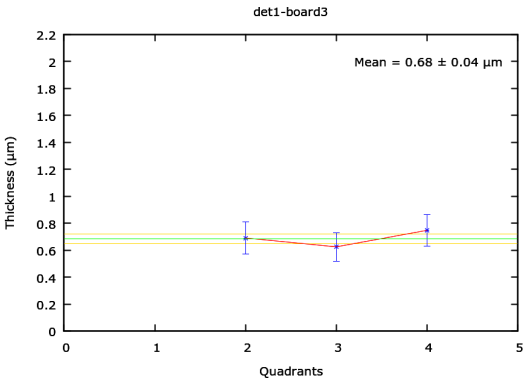
det1-board3
Mean = 0.68 ± 0.04 µm
Thickness (µm)
Quadrants

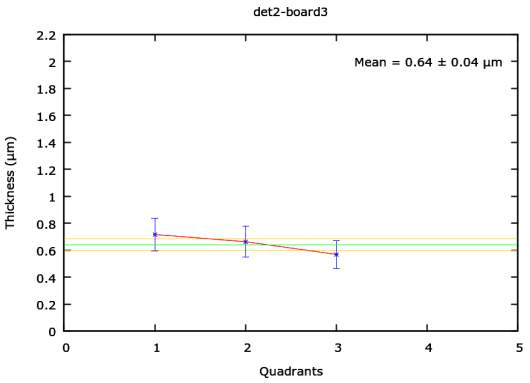
det2-board3
Mean = 0.64 ± 0.04 µm
Thickness (µm)
Quadrants

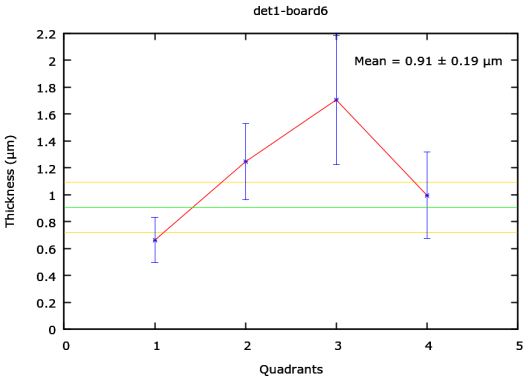
det1-board6
Mean = 0.91 ± 0.19 µm
Thickness (µm)
Quadrants

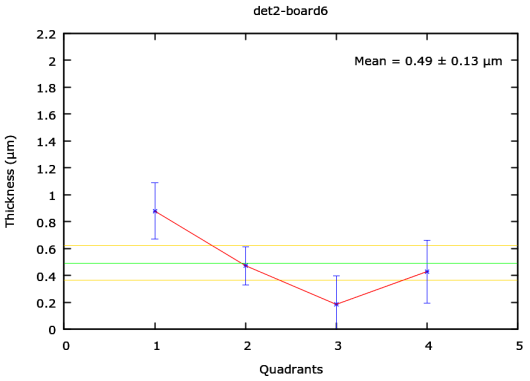
det2-board6
Mean = 0.49 ± 0.13 µm
Thickness (µm)
Quadrants

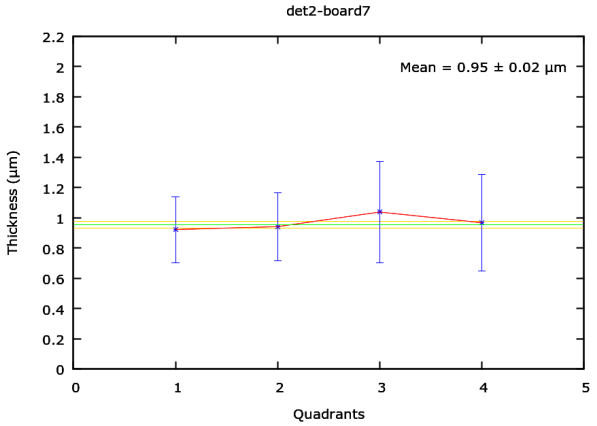
det2-board7
Mean = 0.95 ± 0.02 µm
Thickness (µm)
Quadrants

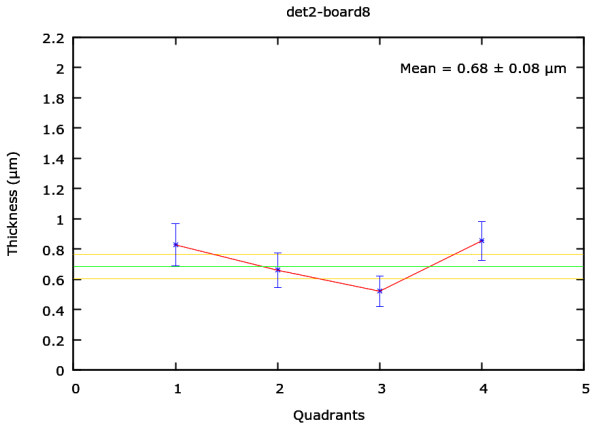
det2-board8
Mean = 0.68 ± 0.08 µm
Thickness (µm)
Quadrants

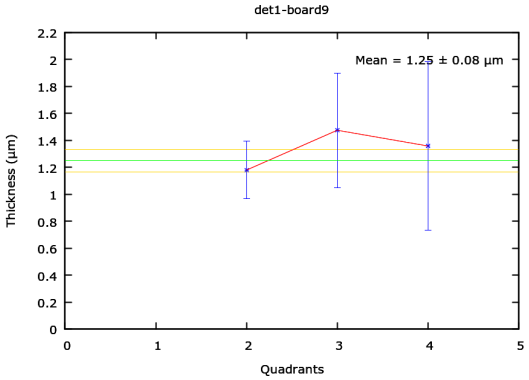
det1-board9
Mean = 1.25 ± 0.08 µm
Thickness (µm)
Quadrants

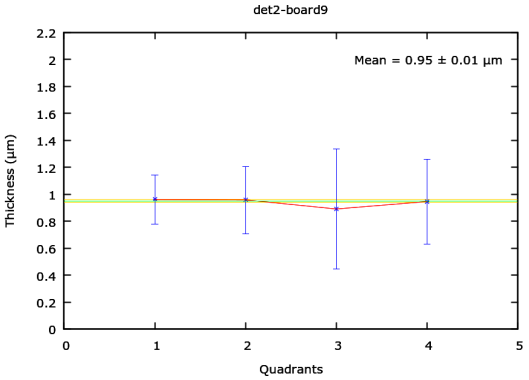
det2-board9
Mean = 0.95 ± 0.01 µm
Thickness (µm)
Quadrants

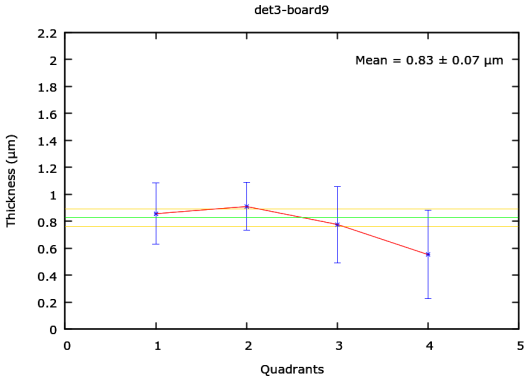
det3-board9
Mean = 0.83 ± 0.07 µm
Thickness (µm)
Quadrants

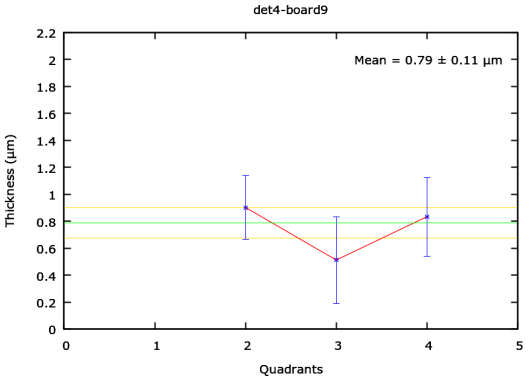
det4-board9
Mean = 0.79 ± 0.11 µm
Thickness (µm)
Quadrants

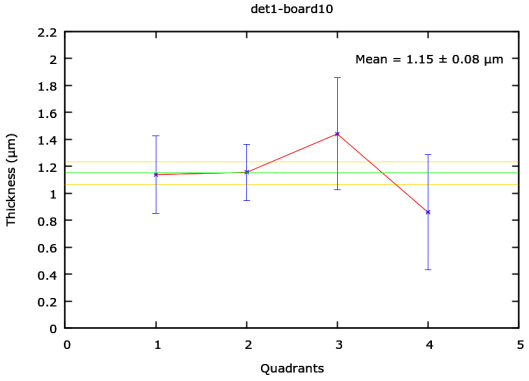
det1-board10
Mean = 1.15 ± 0.08 µm
Thickness (µm)
Quadrants

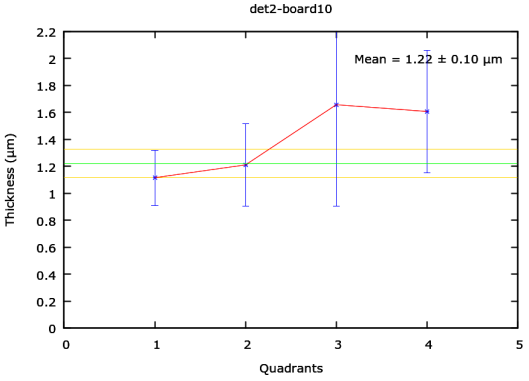
det2-board10
Mean = 1.22 ± 0.10 µm
Thickness (µm)
Quadrants

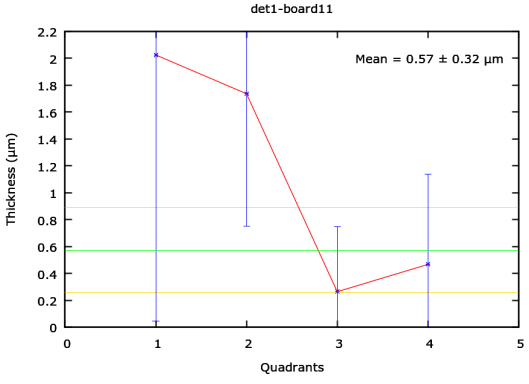
det1-board11
Mean = 0.57 ± 0.32 µm
Thickness (µm)
Quadrants

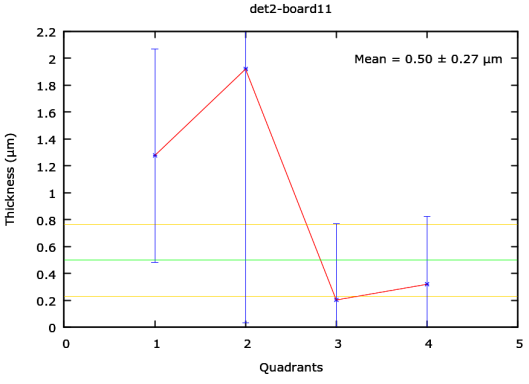
det2-board11
Mean = 0.50 ± 0.27 µm
Thickness (µm)
Quadrants

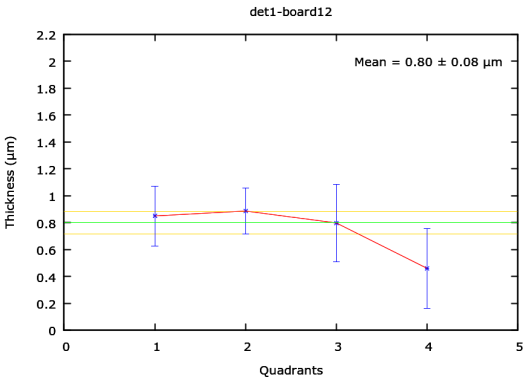
det1-board12
Mean = 0.80 ± 0.08 µm
Thickness (µm)
Quadrants

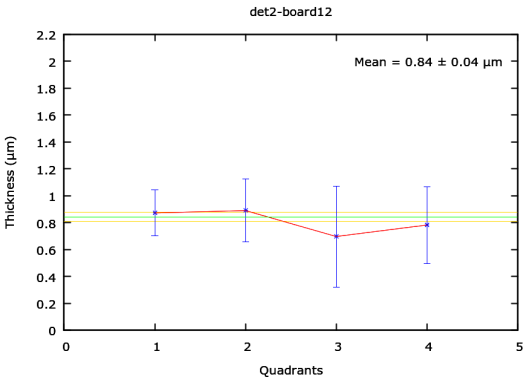
det2-board12
Mean = 0.84 ± 0.04 µm
Thickness (µm)
Quadrants

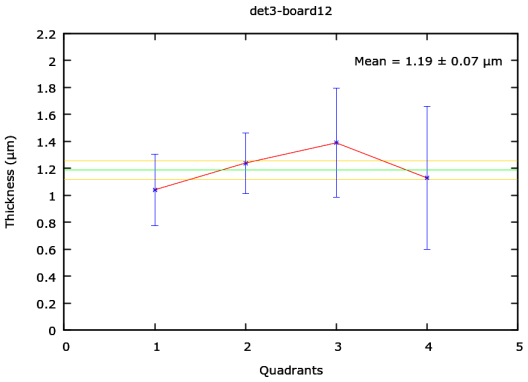
det3-board12
Mean = 1.19 ± 0.07 µm
Thickness (µm)
Quadrants

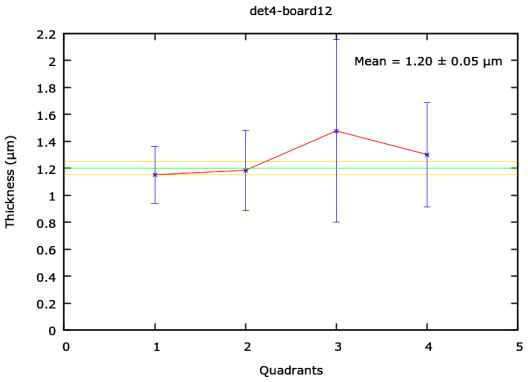
det4-board12
Mean = 1.20 ± 0.05 µm
Thickness (µm)
Quadrants

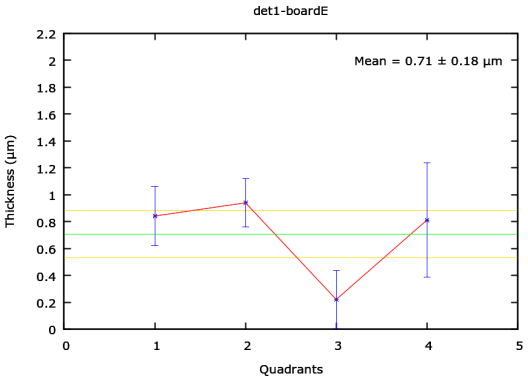
det1-boardE
Mean = 0.71 ± 0.18 µm
Thickness (µm)
Quadrants

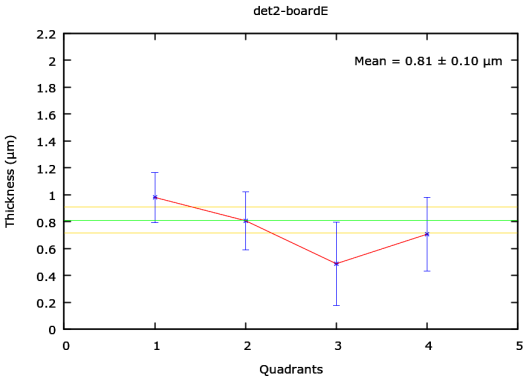
det2-boardE
Mean = 0.81 ± 0.10 µm
Thickness (µm)
Quadrants

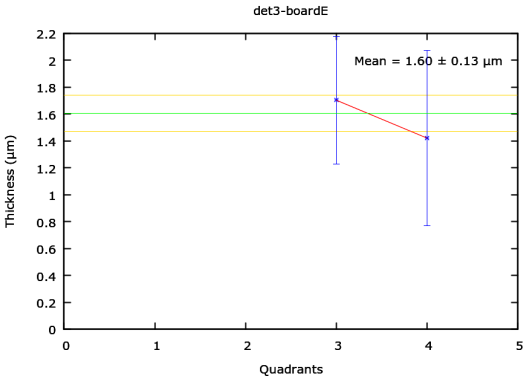
det3-boardE
Mean = 1.60 ± 0.13 µm
Thickness (µm)
Quadrants

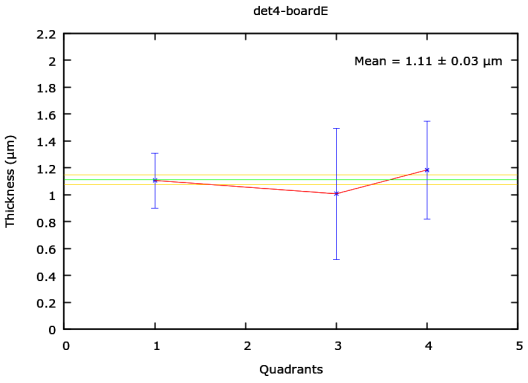
det4-boardE
Mean = 1.11 ± 0.03 µm
Thickness (µm)
Quadrants

Bibliography

[1] L.M. Fraile and J. yst. The {ISOLDE} silicon ball. *Nuclear Instruments and Methods in Physics Research Section A: Accelerators, Spectrometers, Detectors and Associated Equipment*, 513(12):287 – 290, 2003. Proceedings of the 6th International Conference on Position-Sensitive Detectors.

[2] M. Pfützner, M. Karny, L. V. Grigorenko, and K. Riisager. Radioactive decays at limits of nuclear stability. *Rev. Mod. Phys.*, 84:567–619, Apr 2012.

[3] Gerda Pfennig, Christophe Normand, Joseph Magill, Thomas Fanghnel, and Gertrud Weber. *Karlsruher Nuklidkarte: Commemoration of the 50th anniversary.* Marktdienste Haberbeck, Lage, 2008.

[4] http://www.nndc.bnl.gov/. National Nuclear Data Center.

[5] B. Blank and M.J.G. Borge. Nuclear structure at the proton drip line: Advances with nuclear decay studies. *Progress in Particle and Nuclear Physics*, 60(2):403 – 483, 2008.

[6] Antonio C.C. Villari and J.R.J. Bennett. Fast unstable nuclear beam facilities: present and future. *Comptes Rendus Physique*, 4(4):595 – 608, 2003.

[7] I. Tanihata, H. Hamagaki, O. Hashimoto, Y. Shida, N. Yoshikawa, K. Sugimoto, O. Yamakawa, T. Kobayashi, and N. Takahashi. Measurements of interaction cross sections and nuclear radii in the light p-shell region. *Phys. Rev. Lett.*, 55:2676–2679, Dec 1985.

[8] http://www.nap.edu/. The National Academy Press.

[9] J. Meng, H. Toki, S.G. Zhou, S.Q. Zhang, W.H. Long, and L.S. Geng. Relativistic continuum hartree bogoliubov theory for ground-state properties of exotic nuclei. *Progress in Particle and Nuclear Physics*, 57(2):470 – 563, 2006.

[10] Nils Paar, Dario Vretenar, Elias Khan, and Gianluca Col. Exotic modes of excitation in atomic nuclei far from stability. *Reports on Progress in Physics*, 70(5):691, 2007.

[11] K. Krane. *Introductory Nuclear Physics.* John Wiley and Sons, 2 edition, 1988.

[12] R. Dilão and Rui Alves-Pires. *Nonlinear Dynamics in Particle Accelerators.* Series in Mathematical Biology and Medicine. World Scientific, 1996.

[13] https://www.cmamuam.es/es/instalaciones. CMAM.

[14] Ricardo Domínguez Reyes. *Emisión de partículas tras la desintegraciín β^+ en núcleos deficientes en neutrones: ^{17}Ne,^{32}Ar y ^{33}Ar.* PhD thesis.

[15] http://www.lhc-facts.ch/. CERN.

[16] http://isolde.web.cern.ch/.

[17] H. O. U. Fynbo et al. The β 2p decay mechanism of ^{31}Ar. *Nucl. Phys.*, A677:38–60, 2000.

[18] M Oinonen, G Bollen, O Engels, F Herfurth, A G Kellerbauer, H J Kluge, S Schwarz, C Weber, J yst, J Cederkll, H O U Fynbo, U Kster, T Nilsson, T Siiskonen, L Weissman, A Jokinen, J Huikari, V Kolhinen, A Nieminen, J Szerypo, H Schatz, and H L Ravn. Nuclear binding around the rp-process waiting points ^{68}Se and ^{72}Kr. Technical Report CERN-INTC-2000-044. INTC-135-[SIC!]. INTC-I-035, CERN, Geneva, Nov 2000.

[19] T. Nilsson, G. Nyman, and K. Riisager. Halo-nuclei at isolde. *Hyperfine Interactions*, 129(1):67–81, 2000.

[20] G. F. Knoll. *Proportional Counters.* Wiley, 3rd edition, 1999.

[21] Frank Hartmann. *Evolution of silicon sensor technology in particle physics.* Springer, 2009.

[22] S.M. Sze. *Physics of Semiconductor Devices.* Wiley-Interscience publication. John Wiley & Sons, 1981.

[23] Frank Hartmann. Silicon tracking detectors in high-energy physics. *Nuclear Instruments and Methods in Physics Research Section A: Accelerators, Spectrometers, Detectors and Associated Equipment*, 666:25 – 46, 2012. Advanced Instrumentation.

[24] http://www.micronsemiconductor.co.uk/. Micron Semiconductor Ltd.

[25] http://www.mesytec.com/. Mesytec.

[26] http://www.caen.it/. CAEN.

[27] http://www.mvme.com/. Innovative Research Technologies (Motorola).

[28] http://www.mesytec.com/products/nuclear-physics/mpr-16.html. Mesytec Pre-Amplifier mocule MPR-16.

[29] http://www.mesytec.com/products/datasheets/stm-16+.pdf. Mesytec Amplifier module STM-16.

[30] http://www.caen.it/csite/caenprod.jsp?parent=12&idmod=106. CAEN Logic module FAN-IN/FAN-OUT N454.

[31] http://www.caen.it/csite/caenprod.jsp?idmod=114&parent=12. CAEN logic module N405.

[32] http://www.caen.it/csite/caenprod.jsp?parent=12&idmod=385. CAEN Logic module NIM-ECL Translator N638.

[33] http://www.caen.it/csite/caenprod.jsp?idmod=24&parent=11. CAEN scaler module V830.

[34] http://www.caen.it/jsp/template2/caenprod.jsp?parent=12&idmod=299. CAEN gate and delay generator module N1145.

[35] http://www.caen.it/csite/caenprod.jsp?parent=11&idmod=37. ADC from CAEN.

[36] http://www.caen.it/jsp/template2/caenprod.jsp?parent=11&idmod=785. CAEN TDC module V1190A.

[37] http://www.caen.it/jsp/template2/caenprod.jsp?parent=12&idmod=98. CAEN dual timer module N93B.

[38] H. Postema B. Verlaat, A.P. Colijn. The future of co2 cooling in particle physics detectors. *23th International Conference of Refrigeration : Refrigeration for Sustainable Development*, 2011.

[39] B.L. Wall, J.F. Amsbaugh, A. Beglarian, T. Bergmann, H.C. Bichsel, L.I. Bodine, N.M. Boyd, T.H. Burritt, Z. Chaoui, T.J. Corona, P.J. Doe, S. Enomoto, F. Harms, G.C. Harper, M.A. Howe, E.L. Martin, D.S. Parno, D.A. Peterson, L. Petzold, P. Renschler, R.G.H. Robertson, J. Schwarz, M. Steidl, T.D. Van Wechel, B.A. VanDevender, S. Wstling, K.J. Wierman, and J.F. Wilkerson. Dead layer on silicon pin diode charged-particle detectors. *Nuclear Instruments and Methods in Physics Research Section A: Accelerators, Spectrometers, Detectors and Associated Equipment*, 744:73 – 79, 2014.

[40] http://www.mesytec.com/products/nuclear-physics/mhv-4.html. Mesytec power supply module MHV-4.

[41] http://npg.dl.ac.uk/midas/. MIDAS.

[42] Rene Brun and Fons Rademakers. ROOT - An object oriented data analysis framework. *Nuclear Instruments and Methods in Physics Research Section A: Accelerators, Spectrometers, Detectors and Associated Equipment*, 389(1-2):81 – 86, 1997. New Computing Techniques in Physics Research V.

[43] J. F. Ziegler and J. P. Biersack. http://www.srim.org/. SRIM - The Stopping and Range of Ions in Matter.